https://doi.org/10.5194/egusphere-2026-7112
Preprint. Discussion started: 25 November 2026
© Author(s) 2026. CC BY 4.0 License.

Geometry-controlled meridional transport as a physical interpretation of threshold deglaciations: A 1-ODE Conceptual Model of Glacial–Interglacial Cycles

Enrico Maiero[1], Filippo Giorgi[2], and Cosimo Solidoro[1]

[1]Istituto Nazionale di Oceanografia e di Geofisica Sperimentale (OGS), Borgo Grotta Gigante 42/c, 34010 Sgonico (TS), Italy
[2]The Abdus Salam International Centre for Theoretical Physics (ICTP), Trieste, Italy

Correspondence: Enrico Maiero (emaiero@ogs.it)

Abstract. We present a one-equation conceptual model of Late Pleistocene glacial–interglacial cycles, in which the position of the Northern Hemisphere ice-sheet margin evolves under orbital forcing through the competing effects of snowfall, local insolation-driven ablation, and meridional heat and moisture transport.

Rather than being prescribed as jumps between discrete states, the size dependence of the deglaciation threshold emerges from the interaction between orbital forcing and a transport term that strengthens as the ice sheet expands towards lower latitudes, providing a physical interpretation of the threshold behaviour introduced phenomenologically by Paillard (1998). The moisture and heat transport terms depend on the meridional temperature gradient between the tropics and the ice-sheet margin, thereby controlling how the deglaciation threshold varies with ice-sheet size. Additional nonlinear feedbacks associated with ice-sheet retreat are represented through a history-dependent instability amplifier, reproducing the observed asymmetry between slow glaciations and rapid terminations.

After calibration against the LR04 benthic oxygen-isotope stack over the last million years, the model reproduces the timing, amplitude, and irregularity of glacial cycles during the last 800 kyr, with an accuracy comparable to that of Paillard's model while providing an explicit physical interpretation of its switching mechanism. A simple time dependence of two parameters further extends the model to the last two million years and improves its representation of the Mid-Pleistocene Transition.

The results suggest that enhanced meridional heat transport, driven by the amplification of the meridional temperature gradient as the ice sheet expands, may precondition glacial terminations. This mechanism could explain why even relatively weak orbital insolation peaks can trigger deglaciations when Northern Hemisphere ice sheets approach their maximum extent. Further research should focus on a deeper analytical investigation of the model equation, the separation of atmospheric and oceanic transport contributions, its coupling with simplified energy-balance and carbon-cycle equations, and the replacement of phenomenological switches with explicit physical processes. If confirmed, the proposed mechanism would provide a minimal and physically interpretable link between orbital forcing, meridional transport, and nonlinear ice-sheet dynamics throughout Quaternary glacial cycles.

https://doi.org/10.5194/egusphere-2026-7112
Preprint. Discussion started: 25 November 2026
© Author(s) 2026. CC BY 4.0 License.

1 Introduction

Earth's climate during the last few million years has been characterized by the alternation of glacial and interglacial stages (Lisiecki and Raymo, 2005; Imbrie et al., 1993). The main driver of these glacial cycles was identified in the summer insolation forcing on the Northern Hemisphere by Milutin Milanković in the first half of the twentieth century (Milanković, 1941; Hays et al., 1976; Berger, 1978). When summer insolation is weak, the growth of large ice sheets in the Northern Hemisphere is favored, as melting in summer is not intense; on the contrary, when summer insolation is strong, melt is large and snow can hardly survive summers. Summer insolation is controlled by the periodic oscillation of three astronomical parameters that alter Earth's orbit around the Sun, namely obliquity (∼41,000-year periodicity), precession (∼23,000-year periodicity) and eccentricity (∼100,000-year periodicity), although eccentricity is known to have only a secondary *modulating* effect on the precession signal (Berger, 1978).

The relative content of the isotope ^{18}O in benthic foraminifera is the most common proxy for global ice volume and provides a paleoclimate archive that extends back 5.3 million years, most notably in the form of the LR04 stack, a compilation of 57 globally distributed benthic δ^{18}O records aligned by an automated graphic correlation algorithm (Lisiecki and Raymo, 2005). This archive shows that, while in the early Pleistocene (∼2.6–1.2 Ma) the glacial cycles had a main periodicity of about 41,000 years and were limited in amplitude and rather symmetric in time, since the mid-Pleistocene transition (MPT, centered around 900 kyr ago but spanning roughly 1.2–0.7 Ma) the glacial cycles have been characterized by a longer and less regular periodicity (80,000 to 130,000 years), a larger amplitude, and a marked asymmetry in time, alternating a long ice-sheet growth phase with a rapid ice-sheet collapse (about 10,000 years long on average) (Clark and Pollard, 1998).

Several mechanisms have been proposed to explain this transition, and no single hypothesis currently commands consensus (Berends et al., 2021). The *regolith hypothesis* attributes the transition to the progressive glacial erosion of a thick, deformable sediment layer that covered the Laurentide and Fennoscandian shields prior to the Pleistocene: while this regolith was present, it lubricated the ice-sheet base and favored thin, low-amplitude ice sheets that responded linearly to the dominant obliquity forcing; its gradual removal exposed harder crystalline bedrock, increasing basal friction and allowing thicker, more voluminous ice sheets whose response is governed by nonlinear deglaciation dynamics (Clark and Pollard, 1998). A second family of hypotheses instead invokes a long-term decline in atmospheric CO_2 concentration through the Pliocene and early Pleistocene, which would have progressively increased the insolation threshold required to disrupt Northern Hemisphere ice sheets and increased the amplitude of glacial-interglacial swings. Transient Earth-system simulations spanning the last 3 Myr suggest that neither mechanism alone reproduces the observed transition, and that the combined effect of declining CO_2 and regolith removal is required to capture both the amplitude growth and the timing of the 41-to-100-kyr shift (Willeit et al., 2019).

Several conceptual models have been built around these ideas, translating one or more of the proposed physical mechanisms into low-order dynamical systems that can be directly compared against the proxy record. An early and influential example is the relaxation-oscillator model of Imbrie and Imbrie (1980), in which ice volume responds to orbital forcing with an asymmetric response time — faster during deglaciation than during glaciation — foreshadowing the asymmetric relaxation adopted, in different form, by later models including our own. Saltzman and Maasch (1988) and Maasch and Saltzman (1990) instead

https://doi.org/10.5194/egusphere-2026-7112
Preprint. Discussion started: 25 November 2026
© Author(s) 2026. CC BY 4.0 License.

proposed a three-variable system coupling ice volume, atmospheric CO_2, and deep-ocean temperature, in which a free (self-sustained) oscillation internal to the carbon cycle–cryosphere system, rather than orbital forcing alone, is responsible for the observed periodicities, with orbital forcing acting as a pacemaker on an otherwise self-oscillating system. These early models established two ideas that recur throughout the later literature and in the present work: that the climate system's response to insolation must be nonlinear and state-dependent to reproduce the 100-kyr world, and that at least one internal variable must encode some form of memory of the system's recent history beyond the instantaneous forcing. Pérez-Montero et al. (2025) recently conceived a model that embeds the ice-sheet glaciological dynamics into a mass balance equation forced by insolation; they embedded several feedbacks in their model, but essentially found out that only a threshold-activated dependence of ice albedo on ice age could explain the late-Pleistocene glacial cycles. It needs to be noted that the ice age and the ice volume are not independent, so the use of one can be reconciled to the use of the other.

Since these pioneering studies, the literature on low-order glacial-cycle models has developed along several lines. The threshold-switching framework of Paillard (1998) was refined by making the thresholds depend on the state of the system (Parrenin and Paillard, 2003) and by tying the switching to candidate physical processes, such as sea-ice extent (Gildor and Tziperman, 2000) or the behaviour of the Antarctic ice sheet (Paillard and Parrenin, 2004). A second line of work addressed the Mid-Pleistocene Transition and the asymmetry between slow glaciations and rapid terminations directly, within low-order dynamical frameworks (Tziperman and Gildor, 2003; Daruka and Ditlevsen, 2016; Quinn et al., 2018). Legrain et al. (2023) used a conceptual model of threshold type, with parameters allowed to vary in time, to test whether the Mid-Pleistocene Transition requires an abrupt change or can be explained by a gradual one, and found gradual changes more likely (this is the same kind of hypothesis as the monotonic parameter drift adopted in Sect. 2.5 and discussed in Sect. 5.4, although our drift involves different parameters and is not statistically tested against an abrupt alternative). More recently, conceptual models have been used to test how the choice of insolation forcing affects the simulated cycles (Leloup and Paillard, 2022), to represent ice-sheet dynamics through an explicit mass balance (Pérez-Montero et al., 2025), and to explore the response of glacial cycles to anthropogenic CO_2 emissions (Talento and Ganopolski, 2021). Ganopolski (2024) proposed a generalised Milankovitch theory, based on a hierarchy of models and data analysis and illustrated by a conceptual model derived from the intermediate-complexity model CLIMBER-2. In it, terminations occur when ice sheets exceed a critical size while insolation is rising (a "domino effect"), and the 41-to-100-kyr transition is attributed to a gradual increase of that critical size. The physical meaning of the critical size is attributed to a set of processes (sediment cover, dust, isostasy, marine and proglacial-lake instabilities, CO_2). This supports a size-dependent deglaciation threshold (which in the model presented here is carried by the transport geometry of Eq. 3 and 11, and not by an explicit CO_2 dependence.) Verbitsky and Crucifix (2023) examined whether phenomenological paleoclimate models are consistent with the physical scaling of the processes they represent, and concluded that not all of them are (the model we present is phenomenological in the same sense, with effective switches and an effective Hadley-cell margin as discussed Sect. 5.4, and such a consistency test has not been performed here).

Many of these models, together with the many variants that followed, share a common mathematical skeleton that has since been studied in its own right: low-dimensional relaxation oscillators, often piecewise-smooth or threshold-switched, whose qualitative behaviour (limit cycles, excitable regimes, bifurcations between periodicities) can be analysed with the tools of

https://doi.org/10.5194/egusphere-2026-7112
Preprint. Discussion started: 25 November 2026
© Author(s) 2026. CC BY 4.0 License.

dynamical systems theory independently of the specific physical processes any given model attaches to each term (Ghil, 1994; Crucifix, 2012). This perspective is useful background for the present work, since Sect. 2 introduces a further relaxation-type formulation, and Appendix D makes its relationship to Paillard (1998)'s threshold-switching model analytically explicit rather than only qualitative.

Whatever their internal dynamics, any model of the late-Pleistocene cycles has to reproduce not only the correct periodicity and amplitude of glacial-interglacial swings but also the correct *timing* of terminations relative to orbital phase. A statistical test of termination timing against obliquity phase found that the null hypothesis of independence between terminations and obliquity can be rejected, supporting obliquity as a pacing mechanism for terminations even within the nominally 100-kyr world (Huybers and Wunsch, 2005); later work extended this to show a combined role for precession alongside obliquity (e.g. Tzedakis et al., 2017). This is a stronger and more specific test than matching overall spectral power, and it is the reason why several modelling studies, including ours, have preferred to calibrate models on climatic paleodata (Sect. 3.2).

Conceptual models occupy a useful middle ground between data analysis and full Earth-system simulations. They distil the essential physics into a small number of ordinary or partial differential equations (ODEs or PDEs), making it possible to calibrate parameters against the proxy record and to identify which structural elements are necessary. At the other end of the complexity spectrum, Earth system models of intermediate complexity coupling atmosphere, ocean and cryosphere components (Ganopolski and Calov, 2011) and fully-dynamic thermomechanical 3-D ice-sheet models (Golledge et al., 2014) can reproduce glacial cycles with far greater physical fidelity, at the cost of a parameter space too large, and a computational cost too high, to systematically explore or to attribute specific behaviours to specific mechanisms. Conceptual models trade this physical completeness for tractability: with only a handful of parameters, their behaviour can be fully characterised, their sensitivity to each mechanism isolated, and, as we do in Appendix D, their relationship to other conceptual models made analytically explicit. A landmark in this tradition is the model of Paillard (1998), which relies on three fundamental hypotheses: (i) Earth's climate state in the last two million years is determined by two variables, the summer insolation in the Northern Hemisphere and the global volume of ice (which essentially varies due to the development or retreat of the northern ice sheets), according to the equation:

$$\frac{\mathrm{d}V}{\mathrm{d}t} = \frac{V_R - V}{\tau_R} - \frac{F_p}{\tau_F} \tag{1}$$

where V is the ice volume, $F_p = \frac{1}{2}(F_{orig} + \sqrt{4a^2 + F_{orig}^2})$ a truncated form of the summer insolation in the Northern Hemisphere (F_{orig} being the standardised insolation anomaly, with zero mean and unit variance; F_p is then renormalised to zero mean and unit variance, $a = 1$ as in Paillard (1998)), the other terms are parameters; (ii) there are three possible climate states, interglacial (**i**), mild glacial (**g**) and full glacial (**G**), which differ only in the values of the relaxation volume V_R and of the response times τ_R (τ_F does not change) in Eq. (1), the two parameters that switch across states; (iii) transitions between states are triggered by threshold crossings: **i**→**g** when F_{orig} falls below i_0, **g**→**G** when V exceeds a threshold V_0, and **G**→**i** when F_{orig} exceeds $i_1 > i_0$ (the thresholds are applied to F_{orig}, not to F_p). Between triggers the system remains in its current state, whatever the later evolution of F_p; this persistence generates a hysteresis that prevents a mild glacial from deglaciating at the first insolation maximum.

https://doi.org/10.5194/egusphere-2026-7112
Preprint. Discussion started: 25 November 2026
© Author(s) 2026. CC BY 4.0 License.

Such a framework has proven capable of reproducing the glacial cycles of the last million years with impressive detail, and the last two-million year cycles, too, if the maximum ice volume parameter and background insolation trend are made depend on time. However, Paillard (1998) does not explain the physical mechanisms that would justify the presence of such thresholds, nor the physical mechanisms that onset the glaciations and the glacial terminations.

Later developments of this lineage replaced the fixed thresholds of Paillard (1998) with thresholds that depend on the state of the system. In the model of Parrenin and Paillard (2003), the termination is triggered by a combination of ice volume and insolation, so that larger ice sheets terminate at lower insolation; Tzedakis et al. (2017) showed that the insolation peaks leading to interglacials can be identified by a simple rule involving the time elapsed since the previous termination. These formulations capture an essential feature of the record, namely that the insolation required for a termination decreases as the glacial state grows, but the size dependence of the threshold is prescribed (or fitted) in the relevant phase space, and it is not tied to a physical pathway; the switching between states also remains discrete. The model we present addresses the same feature differently. The size dependence of the trigger follows from a single equation, through a meridional transport term that varies continuously with the geometry of the ice margin (Eq. 3), which yields an explicit trigger insolation F_{trig} that decreases as the ice sheet expands (Eq. 11). The equation still contains piecewise switches (c, d and u), each tied to an identifiable process (Sect. 2), but none of them prescribes the size dependence of the trigger. The memory of the glacial depth, which in those models enters through the elapsed time or the volume threshold, is carried by the cumulative retreat in the amplifier u; and the relation to the piecewise-linear formulation of Paillard (1998) is made explicit analytically (Appendix D). This does not make the model more accurate than the earlier ones (Sect. 4), but it provides a physical hypothesis for the size-dependent threshold that can be tested independently, by diagnosing the transport as a function of ice extent (Sect. 5.1).

In this work, we suggest that the onset of glacial terminations can be triggered even by not-too-high insolation if the ice-sheet extension itself enhances heat transport from low to high latitudes via an increase of the meridional temperature gradient: this would justify the V_0 threshold from Paillard (1998). We further suggest, similarly to other authors (e.g. Crucifix, 2011; Abe-Ouchi et al., 2013; Pérez-Montero et al., 2025), that the asymmetry between terminations and glaciations can be explained by positive feedbacks between ice-sheet retreat and albedo and between ice-sheet growth and ice-sheet stability that would explain the sudden change in parameters between the glacial stage and deglaciation. We formalize our hypothesis with a single ODE with piecewise switches that has the meridional margin of the ice sheet as its only dynamic variable and the Northern Hemisphere summer insolation as the only forcing. We find that this model is able to reproduce the irregular 100 kyr glacial cycles of the last 800,000 years (calibrated over the last 1 million years) and it can be extended back to the last 2 million years if some parameters are explicitly made depend on time, essentially reproducing if not even improving results from Paillard (1998).

We adopt the model of Paillard (1998) as our reference for three reasons. First, it belongs to the same structural class as the present one: a single prognostic equation for one ice-volume variable, forced only by Northern Hemisphere summer insolation, with a handful of parameters, whose coefficients are selected by threshold crossings. With the same forcing, the same target record and comparable complexity, differences in skill and behaviour can be attributed to the mechanism that controls the switching rather than to the number of processes represented or to the choice of forcing. Second, the ice-volume

https://doi.org/10.5194/egusphere-2026-7112
Preprint. Discussion started: 25 November 2026
© Author(s) 2026. CC BY 4.0 License.

threshold V_0 of that model is precisely the feature for which we propose a physical interpretation (Sect. 2.4), so the comparison bears directly on the question addressed here; Appendix D makes the connection between the two formulations explicit. While subsequent single-ODE extensions (e.g. Parrenin and Paillard, 2003) already incorporated linear volume-dependent thresholds, we restrict our quantitative baseline to Paillard (1998) because its fixed threshold V_0 represents the exact discrete feature for which our continuous transport geometry provides a physical derivation. This choice isolates the effect of the geometric trigger mechanism from additional model degrees of freedom. Third, it was extended to the last 2 Myr through a linear drift of some parameters, which is the same strategy we follow (Sect. 2.5), so the 2 Myr comparison is like for like.

2 Methods I - The model

2.1 State variable and forcing

The single prognostic variable $x \in [x_H, 1]$ represents the normalised latitude of the southern margin of the Northern-Hemisphere ice sheet, where $x_H = 0.3$ is the northern boundary of the Hadley cell and $x = 1$ corresponds to a fully deglaciated state for which the margin coincides with the North Pole.

The forcing is the June-21 insolation at 65°N, $F_{\mathrm{dim}}(t)$, normalised to $[0, 1]$ over the full insolation series (-50 to +20 Myr), considered as representative of the summer insolation variations occurring at mid-high latitudes in the Northern Hemisphere:

$$F_n(t) = \frac{F_{\mathrm{dim}}(t) - F_{\mathrm{min}}}{F_{\mathrm{max}} - F_{\mathrm{min}}}, \qquad F_{\mathrm{min}} = 421.7\ \mathrm{W\,m^{-2}}, \quad F_{\mathrm{max}} = 575.0\ \mathrm{W\,m^{-2}}. \tag{2}$$

All insolation values, as well as the minimum and the maximum, were computed with the software provided by Laskar et al. (2004). All values were normalised with the fixed minimum and maximum of the full insolation series used as input (-50 to $+20$ Myr). Hereafter we will drop the subscript n.

2.2 Governing equation

The ice-margin position evolves according to

$$\frac{dx}{dt} = d\,F + u\left[\frac{S\,F}{(x - x_H)^N} + c\,F\,(x - x_H)\right] - \frac{B_1}{(x - x_H)^N} - B_0, \tag{3}$$

where $x - x_H$ is the distance of the ice margin x from the Hadley boundary x_H. This equation is a volume balance equation (under the simplifying assumption that the ice-sheet extent is proportional to the ice-sheet volume): all negative terms contribute to increase the ice volume, thus diminishing x, whereas all positive terms increase x and reduce the ice volume. A key idea to this model is that **the meridional transport is inversely proportional to** $(x - x_H)$, because it is directly proportional to the temperature gradient between the tropics and the ice margin. The Hadley-cell margin was chosen, instead of the equator, because the Hadley cell is known for showing rather uniform temperatures; moreover, the ice-sheet margin stays at 0°C by definition at a first approximation, so it can be used instead of the North Pole. So, the five structural terms are:

B_0 *Background build.* A constant build rate independent of ice-margin position (note that the sign can be reversed and this term may become a background destruction).

https://doi.org/10.5194/egusphere-2026-7112
Preprint. Discussion started: 25 November 2026
© Author(s) 2026. CC BY 4.0 License.

$B_1(x - x_H)^{-N}$ *Meridional moisture transport.* As x decreases, the moisture transport from low to high latitudes increases. It is known that such mass contribution to the ice sheets is mainly responsible for their growth at their full development, as highlighted in the case of Antarctica (Delaygue et al., 2000; Sodemann and Stohl, 2009).

$SF(x - x_H)^{-N}$ *Insolation-driven heat transport.* As x decreases, the heat transport from low to high latitudes increases, enhancing the margin retreat by melt, if transport is atmospheric, or by calving or sub-shelf erosion, if transport is marine. Here F, the summer insolation at 65°N, is used as a single proxy for the thermal forcing of the meridional gradient: it drives the temperature of the ice margin and, through large-scale coupling with lower latitudes, that of the Hadley-cell boundary. It is not meant to represent tropical insolation, whose orbital phasing differs. This term encompasses both atmospheric and oceanic heat transport, as both are driven by temperature gradients. In principle, the exponent of this term could be different from N, but attempts in that direction did not lead to effective improvement.

$cF(x - x_H)$ *Local insolation–albedo feedback.* The parameter c controls how strongly the local surface energy balance responds to insolation via albedo. This term introduces a discontinuity with a threshold mechanism, as the parameter c takes two values depending on whether insolation exceeds an insolation threshold F_0:

$$c = \begin{cases} C_2 & \text{if } F \geq F_0 \text{ (strong insolation)}, \\ C_1 & \text{if } F < F_0 \text{ (weak insolation)}, \end{cases} \tag{4}$$

with $C_1 < C_2$. This encodes the physical idea that albedo decreases suddenly if the snow melts. Melting is a threshold-driven mechanism: snow melts if and only if the skin temperature is greater than 0°C. So, in a two-equation model, this condition would be controlled by temperature, but in a one-equation model the best replacement to temperature is insolation. For $F < F_0$ the coefficient C_1 is negative in the calibrated solution: below the melting threshold, stronger summer insolation warms the margin without melting it, and is assumed to favour summer snowfall and a fresh, high-albedo snow cover at the margin, which reduces the local ablation drive. This is a local, sub-threshold effect at the margin, distinct from the large-scale moisture transport represented by B_1. When $F \geq F_0$ the snow melts, the albedo drops and the coefficient switches to $C_2 > C_1$. C_1 is an effective net coefficient combining local accumulation and ablation sensitivities proportional to $F(x - x_H)$; its accumulation and ablation components cannot be separated by the calibration (Appendix E). This term grows with x, given that a progressive decrease in marginal albedo during glacier retreat is supported by melt-induced surface darkening and radiative feedback mechanisms (e.g. Paul et al., 2004; Oerlemans et al., 2009; Tedesco et al., 2016).

dF *Interglacial inertia.* Active only when $x = 1$ ($d = D$ if $x = 1$, else $d = 0$), it makes it harder for glaciation to start when deglaciation is full. This term introduces a physically justifiable threshold mechanism, too. Since it must oppose the onset of glaciation, D is constrained to $D \geq 0$: a negative value would accelerate glacial inception, contradicting the definition of the term.

To ensure mathematical well-posedness in continuous time, Eq. (3) is understood as a projected dynamical system on the state domain $[x_H, 1]$. Specifically, at the deglaciated upper barrier $x = 1$, the velocity is constrained to $\dot{x} = \min(0, \text{RHS})$. When

https://doi.org/10.5194/egusphere-2026-7112
Preprint. Discussion started: 25 November 2026
© Author(s) 2026. CC BY 4.0 License.

pinned at $x = 1$, the constrained velocity $\dot{x} = 0$ places the system on the glaciating branch ($u = 1$; it also resets $x_{\min} = 1$ – see Sect. 2.3), so that any subsequent inception requires RHS < 0.

An objection can be raised against the presence of the insolation forcing F in the heat transport term $S\,F\,(x - x_H)^{-N}$ and its absence in the moisture term $B_1\,(x - x_H)^{-N}$: through the Clausius–Clapeyron relation, atmospheric moisture also depends on temperature and hence, indirectly, on F. The two terms have the same dependence on x, so retaining the dependence on F would not introduce a new term, but would add a contribution $-B_1\,\alpha\,(\mathrm{d}T_H/\mathrm{d}F)\,F\,(x - x_H)^{-N}$ (where α is the fractional Clausius–Clapeyron moisture sensitivity to temperature and T_H is the temperature at the Hadley-cell boundary), corresponding to a fraction $\epsilon = B_1\,\alpha\,(\mathrm{d}T_H/\mathrm{d}F)/S$ of the heat-transport term, with the opposite sign (Appendix E). Neglecting this contribution is therefore an approximation, justified quantitatively if $|\epsilon| \ll 1$, i.e. if the sensitivity of moisture transport to F is small compared with that of heat transport.

This approximation is physically plausible for three reasons. First, the sensitivity of the moisture flux to T_H need not follow the Clausius–Clapeyron relation, since the global hydrological cycle is constrained by the atmospheric energy budget (Allen and Ingram, 2002; Held and Soden, 2006). Second, progressive condensation along air-mass trajectories can deplete the moisture available for snowfall over the cold ice-sheet interior, so that accumulation depends on the history of moisture uptake and precipitation during transport, and only partially on the source temperature (Sodemann et al., 2008). Third, F represents the summer insolation anomaly, to which ablation at the ice-sheet margin responds directly; ablation is also thresholded at the melting point. Snow accumulation over the ice-sheet interior, in contrast, integrates moisture supply and precipitation throughout the year. Model and Lagrangian-diagnostic studies of present-day Antarctica indicate that snowfall over high, cold ice-sheet interiors is supplied predominantly by moisture from mid-latitude oceanic sources (Delaygue et al., 2000; Sodemann and Stohl, 2009; Gao et al., 2024). If a similar source geometry applied, by analogy, to the Northern Hemisphere ice sheets at glacial maxima, accumulation would depend partly on source regions where precession produces large seasonal insolation changes but little change in annual-mean insolation at a fixed latitude. Obliquity also modifies annual-mean insolation, but, owing to the latitudinal structure of the insolation response, its effect on the annual-mean temperature of mid-latitude moisture sources need not be as pronounced as its effect on high-latitude summer conditions. These considerations suggest that annual accumulation may be less sensitive to summer insolation than marginal ablation, although the extent of this difference depends on the seasonal response of evaporation, moisture transport, and precipitation. They motivate, but do not quantitatively establish, a reduced sensitivity of the moisture-transport term to F relative to that of the heat-transport term.

The factors u, c and d are piecewise functions of F, x and $\dot{x}$; their threshold behaviour is not *ad hoc*, but has a physical explanation. We already described $c(F)$ and $d(x)$; in the next section, we will have a closer look at the dependencies of u.

2.3 Instability amplifier

All destruction terms in Eq. 3 are amplified by a multiplicative factor u during deglaciation:

$$u = \begin{cases} \exp\left[U\,(x - x_{\min})^{M_u}\right] & \text{if } \dot{x}(t^-) > 0 \text{ (deglaciating)}, \\ 1 & \text{otherwise (glaciating)}. \end{cases} \tag{5}$$

https://doi.org/10.5194/egusphere-2026-7112
Preprint. Discussion started: 25 November 2026
© Author(s) 2026. CC BY 4.0 License.

Here $x_{\min}$ is the minimum x reached during the current glacial cycle: it is reset to and follows x whenever $\dot{x} < 0$ (glaciating), and it is frozen at the local minimum when $\dot{x}$ reverses to $\dot{x} > 0$ (deglaciating). The quantity $x - x_{\min} \geq 0$ is thus the cumulative retreat since the glacial maximum of the current cycle. The exponent M_u controls whether the argument of the exponential, that controls instability, grows sub-linearly ($0 < M_u < 1$), linearly ($M_u = 1$), or super-linearly ($M_u > 1$) with cumulative retreat. So, u is the memory term of our model: it remembers the last maximum extension of the ice sheet and it is aware of the condition of growth or retreat of the ice sheet. Formally, in continuous time, there is a retreat-mode indicator $w(t) \in \{0, 1\}$ that operates as a two-state relay: it switches from $0 \to 1$ (freezing $x_{\min}$ at the current local minimum) as soon as the unamplified right-hand side (RHS evaluated with $u = 1$) becomes strictly positive, and it switches back from $1 \to 0$ (resetting $x_{\min} = x$ and $u = 1$) when the amplified RHS becomes non-positive (RHS ≤ 0) or when $x = 1$. This continuous-time relay formulation guarantees that the local memory $x_{\min}$ tracks the most recent local turning point of the current cycle, preventing ambiguity at smooth turning points.

The key physical interpretation is that u encodes the increased vulnerability of the ice sheets while retreating: in the first stages of retreat, the margin is often marine, so the ice sheet is subject to instability mechanisms such as Marine Ice Sheet Instability (MISI, Joughin et al. (2012); DeConto and Pollard (2016)) and Marine Ice Cliff instability (MICI, Joughin et al. (2012); DeConto and Pollard (2016)), which are structural instabilities due to the sudden removal of large portions of the margins; then, when the ice sheet is in the late stages of its retreat, its margins are usually continental and hardly covered with fresh snow during summer, thus showing a low albedo (e.g. Shaw et al., 2021; Ren et al., 2024; Tedesco et al., 2016; Shimada et al., 2016; Cook et al., 2020). u can also account for the feedback between temperature and CO_2, as global temperatures show the same trends as the ice volume; it can also account for the melt-elevation feedback and for the isostasy feedback. Because $x_{\min}$ resets at each cycle, each glaciation builds its own instability from scratch, preventing shallow glacials from inheriting the deep $x_{\min}$ of a previous, larger glaciation. This is another key idea to this model: **the ice retreat is faster if the ice sheet is larger** at its peak extension, which is a deep reinterpretation of one of Paillard (1998)'s thresholds. An interpretation of this mechanism comes from the observation that as the ice expands it also thickens, but, roughly speaking, when it retreats it keeps its thickness, so the thickness acts as a memory of its former expansion.

It may look like c from Eq. 4 and u from Eq. 5 are redundant in the $ucF(x - x_H)$ term, but they are not: u is a memory term that accounts for positive feedbacks during the retreat stage of the ice sheet, whereas c only depends on insolation. More specifically, when albedo comes to play, u accounts for the lowering albedo due to dust, lack of fresh snow, etc., whereas c accounts for the lowering of albedo due to the presence of liquid water.

2.4 The transport-driven termination mechanism

Before describing the termination mechanism itself, it is worth noting how the balance of terms in Eq. (3) shifts between large and small $(x - x_H)$, since this shift is plausibly what allows transport, rather than the local terms, to be responsible for the sharp glacial-interglacial transitions described below. For large x (small ice sheets, close to full deglaciation), the transport terms $B_1 (x - x_H)^{-N}$ and $S F (x - x_H)^{-N}$ are small, and the balance is effectively between the constant background build B_0 and the local term $u c F (x - x_H)$.

https://doi.org/10.5194/egusphere-2026-7112
Preprint. Discussion started: 25 November 2026
© Author(s) 2026. CC BY 4.0 License.

During the long glaciation phase ($\sim$80 kyr, with $u = 1$ and $c = C_1 < 0$), ice-sheet growth ($\dot{x} < 0$) is primarily driven by the constant background build B_0, reinforced by the local glaciating term $C_1 F(x - x_H) < 0$. Although the moisture transport term $B_1(x - x_H)^{-N}$ increases as the ice sheet expands, its calibrated magnitude ($B_1 \approx 1.71 \times 10^{-4}$ kyr^{-1}) accounts for only roughly 1.5%–6% of the background accumulation over the physical domain $x \in [0.5, 1.0]$. Crucially, because the ratio $B_1/S \approx 0.024$ is small compared to normalized insolation ($F > 0.07$ throughout the record), the net transport combination $(SF - B_1)(x - x_H)^{-N}$ remains positive (deglaciating) even during glaciation. Ice-sheet buildup proceeds because $B_0 + |C_1| F(x - x_H)$ exceeds $(SF - B_1)(x - x_H)^{-N}$. As the ice margin approaches lower latitudes (small $x - x_H$), the non-linear scaling of $(x - x_H)^{-N}$ progressively amplifies the insolation-driven heat transport $SF(x - x_H)^{-N}$, until it eventually overcomes the net accumulation and initiates a sign reversal of $\dot{x}$.

A key novelty of the present model is that terminations are not prescribed events but emerge from the interplay between four terms in Eq. (3): the heat and moisture transport terms $SF(x - x_H)^{-N}$ and $B_1(x - x_H)^{-N}$, that shape the conditions for the termination to start, and the instability amplifier u and the local albedo amplifier c, that sustain the terminations (c is also involved in triggering the minor terminations).

During a deep glacial state, the ice margin is at low latitude (small $(x - x_H)$), where $(x - x_H)^{-N}$ is large. The transport term $SF(x - x_H)^{-N}$ therefore provides a strong insolation-driven melt flux at the margin. When F rises above F_0, the local feedback switches to the deglaciating value $C_2 > 0$, adding a further positive drive. Any small retreat (x increases slightly from its glacial minimum $x_{\min}$) causes $u = \exp[U(x - x_{\min})^{M_u}]$ to grow, amplifying *both* the transport term and the local feedback simultaneously. The net effect is a runaway: once retreat begins and insolation is sufficiently high, the system accelerates away from the glacial state at a rate that grows exponentially with cumulative retreat.

This mechanism can be contrasted with the Paillard model in physical terms. In Paillard, the transition $G \to i$ in the parameters τ_R and V_R is instantaneous when $F > i_1$: there is no specification of how the transition occurs, only that it does. In the present model, such a transition is determined by a sign reversal of $\frac{\mathrm{d}x}{\mathrm{d}t}$, which is reached continuously through changes in the ice volume and in the insolation forcing, and only afterwards triggers non-linear, though generally continuous, amplifications, whose *speed* and *amplitude* of the subsequent deglaciation are determined by the state of the system at the time of triggering. Specifically, from a deeper glacial (smaller $x_{\min}$), the transport term $SF(x - x_H)^{-N}$ is larger (because $(x - x_H)$ is smaller), u can reach larger values over the course of the retreat (because $x - x_{\min}$ can span a larger range), and the termination is consequently more rapid and complete. This state-dependence is absent in the Paillard formulation and is a direct consequence of making the transport geometry explicit. It is also consistent with the fact that deeper glacials tend to end in larger retreats (Fig. 1); we note that the upper envelope of this relation is partly set by the roughly constant level of the interglacial δ^{18}O.

The per-cycle reset of $x_{\min}$ (Sect. 2.3) is essential to this mechanism. Without the reset, $x_{\min}$ retains the value from the deepest glaciation in the entire record, so every subsequent cycle — regardless of how shallow — inherits the same instability potential and produces a full termination. The reset ensures that the instability is calibrated to the depth of the *current* glaciation, suppressing spurious terminations from mid-volume glacials while preserving the correct response from deep ones. In dynamical-systems terms, the reset introduces a form of *cycle-dependent memory*: each glaciation sets its own instability threshold.

https://doi.org/10.5194/egusphere-2026-7112
Preprint. Discussion started: 25 November 2026
© Author(s) 2026. CC BY 4.0 License.

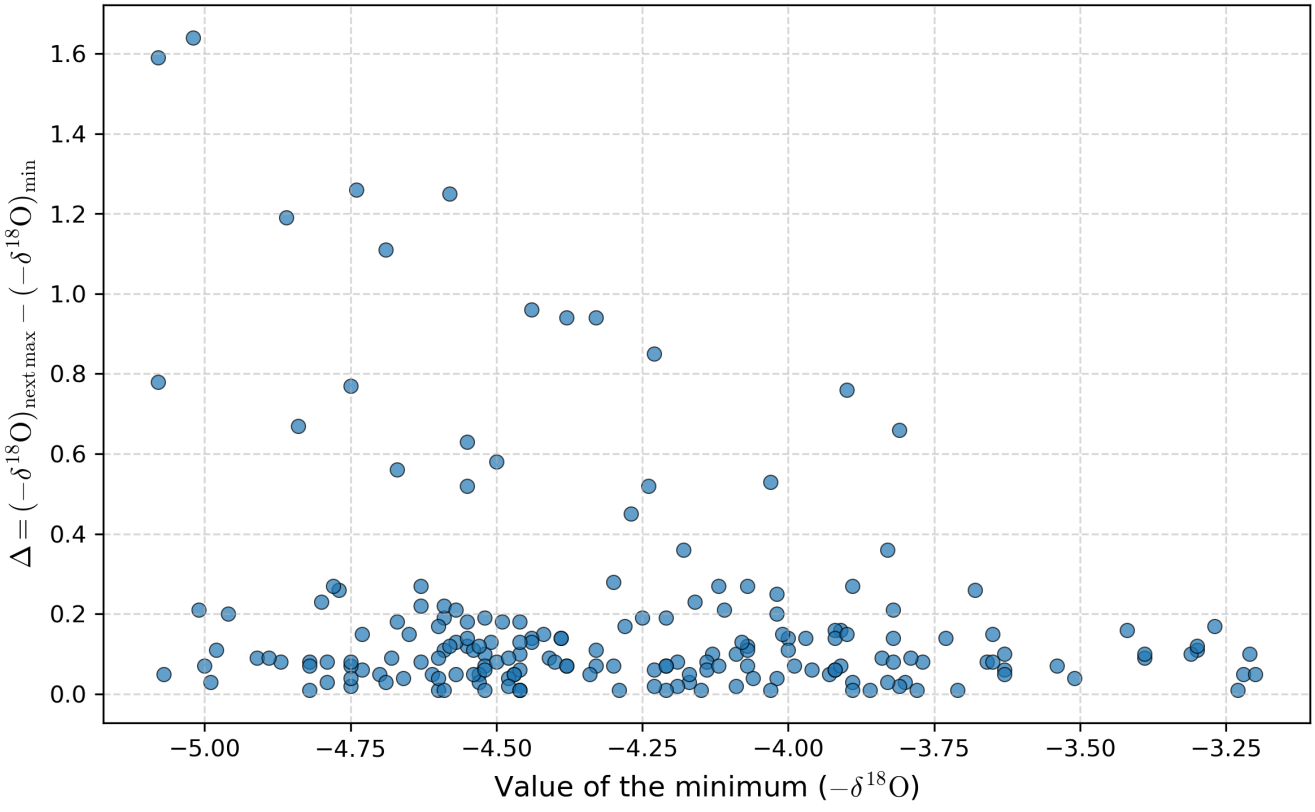

Figure 1. Amplitude of isotopic transitions (Δ) versus initial minimum values for the LR04 benthic δ^{18}O stack over the last 1 Myr (0–1000 ka). Scatter plot comparing local minima of the sign-inverted record ($-\delta^{18}\mathrm{O}_{\mathrm{min}}$, horizontal axis) against the amplitude to the subsequent local maximum (Δ, vertical axis). Peak detection was applied to the sign-inverted series without prominence filtering or smoothing. Transition amplitudes are defined as $\Delta = (-\delta^{18}\mathrm{O})_{next\,max} - (-\delta^{18}\mathrm{O})_{min}$, corresponding to $\delta^{18}\mathrm{O}_{local\,max} - \delta^{18}\mathrm{O}_{next\,min}$ in original isotopic values ($\Delta > 0$). All values are per mil.

To summarise, the physical picture is as follows:

1. Slow glaciation ($d = 0$, $u = 1$, mostly $c = C_1$): the ice sheet grows over $\sim$80 kyr as constant background accumulation B_0 (assisted by local cooling $C_1 F(x - x_H)$) exceeds insolation-driven transport melt.

2. Sign reversal of $\frac{\mathrm{d}x}{\mathrm{d}t}$: for deep glaciations (small $x - x_H$), transport heat melt $S F (x - x_H)^{-N}$ grows sufficiently to balance total accumulation, triggering retreat even if $F < F_0$; for shallower glaciations, retreat is initiated when $F \geq F_0$ and the local feedback switches to $C_2 > 0$, adding a positive drive at the margin.

3. Explosive retreat: the first small retreat activates $u > 1$, amplifying both the transport term and the local feedback. For the calibrated exponent $M_u < 1$, the amplification grows very rapidly at small retreat distances (with an initially unbounded

https://doi.org/10.5194/egusphere-2026-7112
Preprint. Discussion started: 25 November 2026
© Author(s) 2026. CC BY 4.0 License.

slope as $x \to x_{\min}^{+}$) before flattening at larger retreat distances (whereas for $M_u = 1$ it grows exponentially with retreat distance), driving a rapid termination of $\sim$6–10 kyr.

4. Reset: when the retreat reverses ($\dot{x} < 0$), $x_{\min}$ is reset to the current x, and the system re-enters the glaciation phase.

This four-phase cycle is the continuous analogue of the Paillard $i \to g \to G \to i$ sequence, with the crucial difference that step 2 has explicit physics rather than an instantaneous state transition.

2.5 Extension to 2 Ma

Following the example of Paillard (1998), we extended the model back in time up to -2 Myr by imposing a linear trend with time of some parameters. This was done because, before the mid-Pleistocene transition (~ -800 kyr; this is different from Paillard (1998), who assumes a linear trend on the entire domain), the δ^{18}O showed a different kind of variability: oscillations had a lower amplitude, a shorter periodicity (dominated by the obliquity cycle) and were more symmetric. We found that the most effective parameters to reproduce such a trend are U, that controls the symmetry of the cycles, and x_H, that controls the meridional extension of the ice sheet. They were made depend linearly on time between the beginning of the record and the mid-Pleistocene transition, according to:

$$\text{if } \; t < -800 \text{ kyr}: \qquad \begin{cases} U &= U_0 + W(t - t_0) \\ x_H &= x_H^0 + Q(t - t_0) \end{cases} \tag{6}$$

where $t_0 = -2000$ kyr, U_0 and x_H^0 are the values at t_0, and $W = (U_* - U_0)/(t_{\text{MPT}} - t_0)$ and $Q = (x_H^* - x_H^0)/(t_{\text{MPT}} - t_0)$ ensure continuity at $t_{\text{MPT}} = -800$ kyr, after which the previous values are restored.

The extension is deliberately minimal. The ten parameters calibrated on the last 1 Myr (Sect. 3.3) are kept fixed, and only two quantities are allowed to vary in time before the MPT: the amplifier strength U and the equatorward limit x_H of the ice sheet. These two were chosen because they act on the two features that distinguish the early Pleistocene (smaller amplitude and more symmetric cycles) and, among the parameters we tried (including S, B_0 and M_u), they gave the clearest improvement. Their values at -2 Myr, $x_H = 0.54$ and $U = \frac{2}{7}U_*$ (with U_* the post-MPT value), were not calibrated: they were set by hand and checked by inspecting the trajectories and the RMS error over -2 to -0.8 Myr. In this extension $x_H(t)$ acts as an effective moving lower asymptote on x rather than as a literal Hadley-cell extent (Sect. 5.4). The integration starts from $x(t_{\text{start}}) = x_{\text{obs}}(t_{\text{start}})$ with $x_{\min} = x(t_{\text{start}})$ and $u = 1$. The ramps are linear in time and join the post-MPT values continuously at -800 kyr. The extension should therefore be read as a demonstration that a monotonic drift of two parameters is sufficient to reproduce the change of regime, not as an estimate of those parameters.

https://doi.org/10.5194/egusphere-2026-7112
Preprint. Discussion started: 25 November 2026
© Author(s) 2026. CC BY 4.0 License.

3 Methods II - Numerical aspects

3.1 Numerical integration

The ODE is integrated on a $\Delta t = 0.01$ kyr grid over -1000 to 0 kyr and is numerically stable when decreasing Δt (see Table A2 in Appendix A). The insolation series is linearly interpolated on the $\Delta t = 0.01$ kyr grid (without smoothing), whereas the model output is compared with the native 1-kyr LR04 samples. All RMS and r values (including $\mathcal{J}$, the Paillard model and the sea-level comparison) refer to this 1-kyr grid.

The state is advanced with an explicit Euler scheme on the Δt-grid of the insolation series; the rate coefficients in Eq. 3 are expressed in kyr^{-1} (x and F are dimensionless), so a step of length Δt (in kyr) multiplies the right-hand side by Δt. After every step x is clipped to $[x_H + 10^{-6}, 1]$, so that the condition $x = 1$ activating d is attained exactly; d is evaluated on x at the beginning of the step.

In discrete time, the retreat flag of Eq. 5 is the sign of the last increment: the model is on the retreat branch at step n if $x_n > x_{n-1}$ (after clipping). u_n is computed from this flag and from $x_{\min}$ at the beginning of the step, and $x_{\min}$ is set to x_{n-1} when the flag switches from glaciation to retreat. This reproduces the relay of Sect. 2.3 with a delay of at most one step.

The integration starts from $x(-1000\text{kyr}) = x_{\text{obs}}(-1000\text{kyr})$, with $x_{\min} = x(-1000\text{kyr})$ and the model initially in the glaciating branch ($u = 1$). When the forcing is low-pass filtered (Sect. 4.2), the filter is spun up with the 100 kyr of insolation preceding the start of the run.

The full implementation used for the results of Table 1 is available at the Code and Data availability statement, together with the input series or instructions to obtain them.

3.2 Observational normalisation

We use the LR04 benthic δ^{18}O stack as a proxy for ice volume for the following reasons. It is the standard reference for the Plio-Pleistocene glacial cycles, and benthic δ^{18}O records were also the target of Paillard (1998), which makes our results comparable with the model we take as reference. It is, moreover, the only continuous record with a homogeneous chronology and resolution spanning the 2 Myr considered here, and, in principle, the entire 5.3 Myr of the stack, so that a single target allows the same equation to be tested across the Mid-Pleistocene Transition. Sea-level reconstructions that are independent of δ^{18}O and continuous do not extend beyond about 0.8 Myr (Spratt and Lisiecki, 2025), while longer sea-level reconstructions (e.g. Rohling et al., 2014; Miller et al., 2020) are largely derived from benthic δ^{18}O itself and would therefore not provide an independent test. We recognise two limitations of this choice: δ^{18}O reflects both ice volume and deep-ocean temperature, and the LR04 age model is in part orbitally tuned, which may affect the phase relationship with insolation (Lisiecki and Raymo, 2005). For the first, we complement the calibration with a comparison against a sea-level reconstruction over the last 798 kyr (Appendix C).

The LR04 δ^{18}O record (Lisiecki and Raymo, 2005) is converted to x_{obs} via

$$x_{\text{obs}}(t) = \text{clip}\left(1 - \frac{\delta^{18}\text{O}(t) - \delta^{18}\text{O}_{\min}}{\delta^{18}\text{O}_{\max} - \delta^{18}\text{O}_{\min}} \times 0.5,\ 0,\ 1\right), \tag{7}$$

https://doi.org/10.5194/egusphere-2026-7112
Preprint. Discussion started: 25 November 2026
© Author(s) 2026. CC BY 4.0 License.

where $\delta^{18}O_{min} = 2.801\,‰$ and $\delta^{18}O_{max} = 4.910\,‰$ are the 1st and 99th percentiles of the entire LR04 series (-5.3 Myr to present), computed on the native-resolution (1-kyr) series before interpolating to the Δt-grid. The same fixed values are used for the 2 Ma extension. Because the lower percentile is set by the warmest intervals of the whole Pliocene–Pleistocene, observed interglacials of the last 2 Myr do not reach $x_{obs} = 1$: the upper bound $x = 1$ is a model limit, not a level attained by the target. The values were mapped within [0.5, 1] (tails above the 99th percentile slightly extending below 0.5) under the hypothesis that the Northern ice sheets do not extend further south than approximately 45° in latitude.

Acknowledging that the LR04 signal, used for calibration (Sect. 3.3), is also influenced by the deep-ocean temperature, we also statistically compared our model results with a mixed sea-level signal reconstruction from Spratt and Lisiecki (2025) to test the robustness of our model (Sect. 4.2 and Appendix C) over the last 798 kyr. The sea-level data were converted to x using a linear transformation onto the x-range of LR04 over the same window (Appendix C).

3.3 Calibration

Parameters are estimated by minimising a penalised RMS objective over the calibration window $[-1000, 0]$ kyr, excluding MIS6 (-200 to -140 kyr) and MIS11 (-430 to -370 kyr) in all terms in the following equation:

$$\mathcal{J} = \mathrm{RMS}_{\mathrm{calib}} + 3\,\mathrm{RMS}_{\mathrm{upper}} + 3\,\mathrm{RMS}_{\mathrm{lower}}, \tag{8}$$

where $\mathrm{RMS}_{\mathrm{upper}}$ is the RMS error on time steps where $x_{obs} > 0.85$ (interglacial periods) and $\mathrm{RMS}_{\mathrm{lower}}$ is the RMS error where $x_{obs} < 0.58$ (deep glacials). To prevent anomalous orbital responses from biasing global parameter estimation, specific stages are excluded from the primary objective function $\mathcal{J}$. $\mathrm{RMS}_{\mathrm{calib}}$ is computed over the $\mathrm{N}_{\mathrm{calib}}$ 1-kyr samples outside the excluded windows; $\mathrm{RMS}_{\mathrm{upper}}$ and $\mathrm{RMS}_{\mathrm{lower}}$ use the samples with $x_{obs} > 0.85$ and $x_{obs} < 0.58$ within the same set, each normalised by the number of samples of its own subset. Solutions are rejected ($\mathcal{J}$ set to a large value) if the simulated margin has a standard deviation below 45% of that of x_{obs}, a range below 0.18, or never extends south of $x = 0.72$. The constraints $C_1 < C_2$ and $D \geq 0$ were imposed on the objective.

MIS 6 (-200 to -140 ka BP) represents the most eccentric stage in terms of model dynamics: despite high summer insolation, full deglaciation is resisted in observations, whereas standard parameter configurations tend to trigger a full retreat; therefore, it is difficult to reproduce this stage in this class of models (Paillard, 1998) and excluding MIS 6 prevents the global calibration from overfitting to this specific anomaly. Conversely, MIS 11 (-430 to -370 ka BP), characterized by exceptionally low orbital eccentricity and flat insolation variance, is excluded from the primary optimization to serve as an out-of-sample test set, evaluating the model's capacity to generalize across weak-forcing regimes. The bounds of the Latin hypercube search (Stage 1) are listed in Table A1 (Appendix A). The asymmetric penalty encourages the model to reproduce both terminations and glacial maxima faithfully.

Calibration uses a three-stage approach:

1. **Latin Hypercube Sampling** (10000 points) over the 10-dimensional parameter space to identify promising regions (bounds are shown in Table A1).

https://doi.org/10.5194/egusphere-2026-7112
Preprint. Discussion started: 25 November 2026
© Author(s) 2026. CC BY 4.0 License.

2. **Nelder–Mead** local optimisation starting from the top candidates plus 25 random perturbations ($\pm 20\%$) around the two best known solutions.

3. Final polish (repeated) with tight convergence tolerances ($\Delta p < 10^{-9}$, $\Delta \mathcal{J} < 10^{-10}$).

The calibration is not a fully automated global optimisation. The Latin hypercube search was repeated from several sets of bounds and starting points, and the local optimisation was restarted from the most promising candidates. Among the resulting solutions, we selected the one that showed the lowest value of $\mathcal{J}$, and we stopped the search when further restarts did not improve substantially the trajectories. The selected set is therefore a good local optimum, not a demonstrated global one: the existence of other, structurally different solutions with comparable error (Table A3) indicates that $\mathcal{J}$ has several minima, and the Hessian analysis below characterises only the neighbourhood of the selected solution.

To extend the 1-ODE model across the Mid-Pleistocene Transition (MPT, $\sim$1.2–0.8 Ma) over a 2 Myr domain, we incorporate a secular linear drift in the background parameter baseline (Sect. 2.5), similarly in the spirit to Paillard (1998), but applied to different parameters. Because this secular trend deterministically governs the non-stationary evolution prior to 1 Ma, systematic parameter sensitivity exploration (such as the Hessian ellipsoid analysis described next) is anchored to the stationary 1-Myr domain, where parameters remain constant.

To test the robustness of the calibration results, we explored a neighborhood of the best-fit solution in the parameter space along the principal directions of sensitivity. Because $\mathcal{J}$ is piecewise smooth due to discrete switches in ablation rates and relay states, the finite-difference Hessian matrix serves primarily to identify the principal sensitivity directions (eigenvectors) rather than a strictly smooth quadratic basin.

The Hessian of $\mathcal{J}$ at the best-fit was computed numerically with central finite differences (second differences on the diagonal and four-point mixed differences off the diagonal), using a relative step $\delta p_j = 0.01\,|p_j|$ for each parameter, with the integration scheme of Sect. 3.1 and parameters in physical units. Along flat parameter directions (such as the interglacial inertia parameter D), an added numerical ridge (10^{-8} times the mean absolute diagonal) guarantees matrix invertibility during eigendecomposition.

The semi-axes of the ellipsoid, initially set by the quadratic estimate (s_{quad}; $s_{\mathrm{quad}} = 5$ for directions with non-positive curvature), were calibrated along each eigenvector by a 24-step bisection with upper bracket $\min(3s_{\mathrm{quad}}, 5)$. A semi-axis is accepted only if both $+s_k \mathbf{v}_k$ and $-s_k \mathbf{v}_k$ keep the maximum relative change of $\mathcal{J}$, RMS and r within 20%. D is clipped to $D \geq 0$ at every evaluation.

Finally, $N = 500$ members were sampled uniformly in the resulting ellipsoid (radius $u^{1/10}$, with u from a one-dimensional Latin hypercube; Gaussian direction). Members with an invalid objective count as outside tolerance. Because of the piecewise-smooth nature of $\mathcal{J}$, the Hessian provides a local orientation of the sensitivity, not an independent measure of robustness.

https://doi.org/10.5194/egusphere-2026-7112
Preprint. Discussion started: 25 November 2026
© Author(s) 2026. CC BY 4.0 License.

4 Results

4.1 Best-fit parameters

Table 1 lists the calibrated parameters for the full 10-parameter model. Two possible parameter sets were selected. The best-fit shows the best metric in both the 1Ma and the 2Ma time series, whereas the MIS6-adaptable set performs better during MIS6 if a smoothing in time for insolation is introduced (see Sect. 4.2). It has to be said that this is not a result of the calibration, but of a preliminary research; nevertheless, we show it here due to this interesting property.

Table 1. Calibrated parameters of the full model, best-fit and MIS6-adaptable. The insolation threshold is actually used in the model only in the normalised form. In the second block the parameters for the 2 Ma extension are shown, which were set by hand.

Symbol	Best-fit	MIS6-adaptable	Physical role
D	0.0001045	0.01183	Interglacial inertia [kyr^{-1}]
U	2.140	5.056	Instability amplifier strength
S	0.007175	0.003725	Insolation–heat-transport coupling [kyr^{-1}]
C_1	−0.008555	−0.004555	Local-albedo feedback (glaciation) [kyr^{-1}]
C_2	0.008275	0.06330	Local-albedo feedback (deglaciation) [kyr^{-1}]
B_0	0.01632	0.01068	Background build [kyr^{-1}]
B_1	0.0001710	0.0002077	Moisture-transport amplitude [kyr^{-1}]
N	1.065	1.258	Power-law geometry
F_0^{dim}	521.3	533.6	C-switching insolation threshold [W m^{-2}]
F_0	0.6501	0.7301	Normalised C-switching insolation threshold
M_u	0.2971	0.1047	Nonlinearity of u
U_0	0.6115	1.445	U at -2Myr
x_H^0	0.54	0.54	x_H at -2Myr
Q	−0.0002	−0.0002	x_H coefficient for time [kyr^{-1}]
W	0.001274	0.003009	U coefficient for time [kyr^{-1}]

The best-fit calibrated solution achieves RMS $= 0.0733$, Pearson $r = 0.7584$ over the full 1Ma record (including MIS6 and MIS11). The insolation threshold $F_0 \approx 521.3\,\mathrm{W\,m^{-2}}$ means that C_2 is active for approximately 14% of the record (high insolation periods), while the small instability exponent $M_u \approx 0.30$ implies that the amplifier u grows rapidly even for modest retreat (sublinear growth of the exponential argument: large sensitivity at small $x - x_{\min}$, saturating as cumulative retreat increases). If the 2 Ma time domain is considered, then RMS $= 0.0656$, $r = 0.7572$.

The MIS6-adaptable calibrated solution achieves RMS $= 0.1649$, Pearson $r = 0.5111$ over the full 1Ma record (including MIS6 and MIS11). The insolation threshold $F_0 \approx 533.6\,\mathrm{W\,m^{-2}}$ means that C_2 is active for approximately 6% of the record

https://doi.org/10.5194/egusphere-2026-7112
Preprint. Discussion started: 25 November 2026
© Author(s) 2026. CC BY 4.0 License.

(high insolation periods). If the 2 Ma time domain is considered, then RMS $= 0.1538$, $r = 0.5052$ and the model is not able to fully catch the shorter periodicity before mid-Pleistocene transition. So, this parameter combination is worse than the best-fit.

We also recreated Paillard's model, using the parameters published in Paillard (1998). The ice volume V of that model, normalised by construction to $[0, 1]$ (clipped to this interval), was converted to the margin variable with the fixed map $x = 1 - V/2$, which spans $[0.5, 1]$ like x_{obs} (Eq. 7, where the factor 0.5 follows the same convention). We found that during the last 1Ma Paillard's model achieves RMS $= 0.0919$, Pearson correlation $r = 0.8039$, whereas for the 2Ma time series the results are RMS $= 0.1642$ and $r = 0.4559$.

Table 2. Skill on LR04, last 1 Myr (1-kyr grid). $\mathcal{J}$ is computed outside MIS6 and MIS11; RMS and r use the full record.

Model	$\mathcal{J}$	RMS	r	RMS (MIS6)	RMS (MIS11)
Transport model	0.2887	0.0733	0.7584	0.1416	0.0631
Paillard, published	0.5367	0.0919	0.8039	0.1737	0.0522
Paillard, recalibrated	0.3139	0.0747	0.7685	0.0923	0.0448

Recalibrating Paillard's model on LR04 with the same objective reduces its RMS by about 19% (RMS = 0.0747, r = 0.7685, Appendix B). On the calibration window, our model has a lower $\mathcal{J}$ (0.289 against 0.314) and a slightly lower RMS (0.0733), whereas the recalibrated Paillard model has a higher correlation and a smaller error in the excluded intervals MIS6 and MIS11 (Table 2). The two models are therefore comparable on the same target; both improve substantially on Paillard's published parameters ($\mathcal{J}$ = 0.537, RMS = 0.0919). On the 2 Ma record our model is better than all Paillard variants (Appendix B). We chose to retain as main reference the original Paillard's model; the results for the recalibrated one are shown in Table 2 and in Appendix B.

In the recalibrated version the switching thresholds (i_0, i_1, V_0) were kept at their published values, since they define the discrete state structure that our continuous formulation is meant to replace; only the five timescale and relaxation parameters were fitted. The recalibrated model therefore has fewer free parameters than ours (5 against 10), and Table 2 should be read as a lower bound on the skill achievable with a threshold model.

4.2 Comparison with the benthic δ^{18}O

As expected from the RMS and r results, our model and Paillard's show a good agreement during the last 1Ma, as both do with observations (Fig. 2). Nonetheless, some differences remain: Paillard's original model tends to reach full deglaciation at each major termination, whereas ours does not; our model anticipates the glacial peak around -800kyr and delays the two glacial peaks before -700kyr, as well as for the partial deglaciation between them and the full one after them (similarly to Paillard). It also predicts a shallower partial deglaciation around -500kyr (and so does the recalibrated Paillard's model, Fig. B1). Both models well reproduce MIS11, although it was excluded from calibration in our case and can be considered a test set for the calibration. Both fail to reproduce MIS6 by predicting a deglaciation that does not take place. In both MIS6 and MIS11 the recalibrated Paillard's model performs better (Table 2). In general, our model shows a rather smooth profile, that

https://doi.org/10.5194/egusphere-2026-7112
Preprint. Discussion started: 25 November 2026
© Author(s) 2026. CC BY 4.0 License.

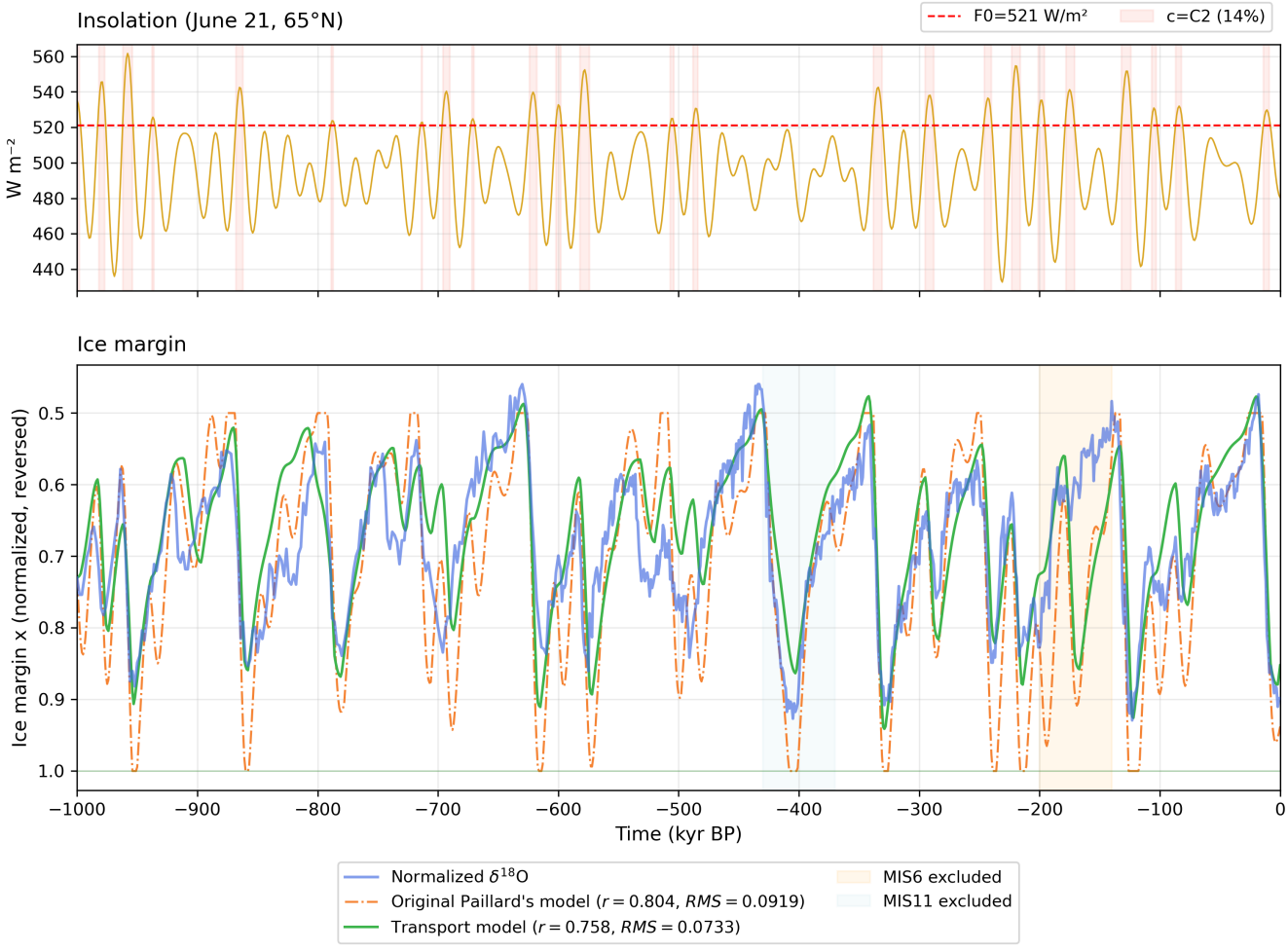

Figure 2. Glacial cycles during the last million years. Top panel shows the insolation forcing, together with the insolation threshold F_0 in use in our model for the switching of the c values; the portions of the series where insolation exceeds such a limit are highlighted. The bottom panel shows in solid blue the δ^{18}O record, converted to x_{obs} according to Eq. 7, in solid green the results of our model with the best-fit parameters, in dashed orange the results from Paillard (1998); the vertical axis uses a reverse scale in order to show the trends in ice volume.

https://doi.org/10.5194/egusphere-2026-7112
Preprint. Discussion started: 25 November 2026
© Author(s) 2026. CC BY 4.0 License.

better represents the alternation of the glacial and interglacial stages, whereas Paillard's better reproduces minor oscillations when they correspond to insolation oscillations.

We also tested the robustness of our model through a statistical comparison with sea-level data from Spratt and Lisiecki (2025) over the last 798 kyr. Over the last 798 kyr, with the sea-level stack mapped onto the same x-range as LR04 (Appendix C, Fig. C1), our model gives RMS = 0.0779,$r = 0.7715$, against RMS = 0.0884, $r = 0.8086$ for Paillard's published parameters and RMS = 0.0889, $r = 0.7338$ for the recalibrated version; on LR04 over the same window the values are 0.0731 and 0.7674 for our model. Pearson r does not depend on the scaling. The sea-level stack is not completely independent of δ^{18}O, so this is a robustness check and not an independent validation.

As already pointed out in Paillard (1998), MIS6 is very hard to catch with this kind of models, because a very high insolation in that stage was not able to trigger a deglaciation. Several explanations have been proposed for this missing deglaciation. One possibility is that the penultimate glaciation reached an exceptionally stable configuration, requiring a stronger combination of insolation, atmospheric CO_2 concentration and internal ice-sheet feedbacks than represented in conceptual models (Ganopolski and Calov, 2010; Parrenin and Paillard, 2003). Another hypothesis is that delayed isostatic adjustment and the resulting elevation–mass balance feedback inhibited the onset of rapid retreat despite favourable orbital forcing (Abe-Ouchi et al., 2013; Oerlemans, 1980; Whitehouse, 2018). Finally, stochastic internal climate variability and ocean-circulation changes may have delayed the termination beyond what orbital forcing alone would predict (Crucifix, 2012; Ditlevsen, 2009; Tzedakis et al., 2017; Cheng et al., 2009).

We also ran a sensitivity experiment in which the raw insolation forcing $F(t)$ is replaced by a first-order low-pass filtered forcing $F_s(t)$, governed by $\mathrm{d}F_s/\mathrm{d}t = (F - F_s)/\tau$ with an exact exponential update scheme (Fig. 3). The time constant τ was scanned from 0 to 10 kyr (at a pace of 0.1 kyr between 0 and 1 kyr, 0.5 kyr for greater values) and the τ valued that minimised the full 1-Myr objective $\mathcal{J}$ (Eq. 8) was selected, yielding optimal values of $\tau \approx 0.00$ kyr for the calibrated best-fit solution and $\tau = 4.00$ kyr for the MIS6-adaptable solution (such a result is very unstable, though, as for $\tau = 4.5$, $\mathcal{J}$ more than doubles). For the MIS6-adaptable parameter set, while the unfiltered model ($\tau = 0$) overpredicts the amplitude of deglaciations across several cycles, introducing the low-pass filter with $\tau \approx 4.00$ kyr attenuates precession-band peaks by $\sim 32 - 40\%$ and delays them by ~ 3.0 kyr. This opens the possibility that the observed lack of termination at MIS6 may be due to some internal buffering of the climate system, such as an intermediate reservoir (e.g. deep-ocean heat storage, carbon-cycle buffering, or slow ice-sheet/lithospheric thermal response), none of which can be further inspected with the transport model at its current state. This attenuation moderates the excessive retreat amplitudes, bringing the interglacial peaks into better alignment with the observed LR04 stack, while simultaneously lowering the insolation peak during MIS6 below the high threshold $F_0 = 533.58\,\mathrm{W\,m^{-2}}$ ($F_{0n} = 0.7301$) to suppress the spurious deglaciation (RMS_6 drops from 0.2854 at $\tau = 0$ to 0.0711, and overall 1-Myr RMS decreases from 0.1649 to 0.1028, r increases from 0.5111 to 0.7621, $\mathcal{J}$ decreases from 1.097 to 0.5194). For the primary calibrated best-fit solution, $\tau \to 0.00$ kyr ($\mathrm{RMS} = 0.0733$, $r = 0.7584$), confirming that the unfiltered insolation forcing remains optimal for the primary model baseline.

On the 2 Ma record our model shows better metrics than Paillard's for essentially two reasons: it is not pushed towards full deglaciation at each termination (as it is by the model structure in Paillard (1998)), and the evolution in time of U guarantees

https://doi.org/10.5194/egusphere-2026-7112
Preprint. Discussion started: 25 November 2026
© Author(s) 2026. CC BY 4.0 License.

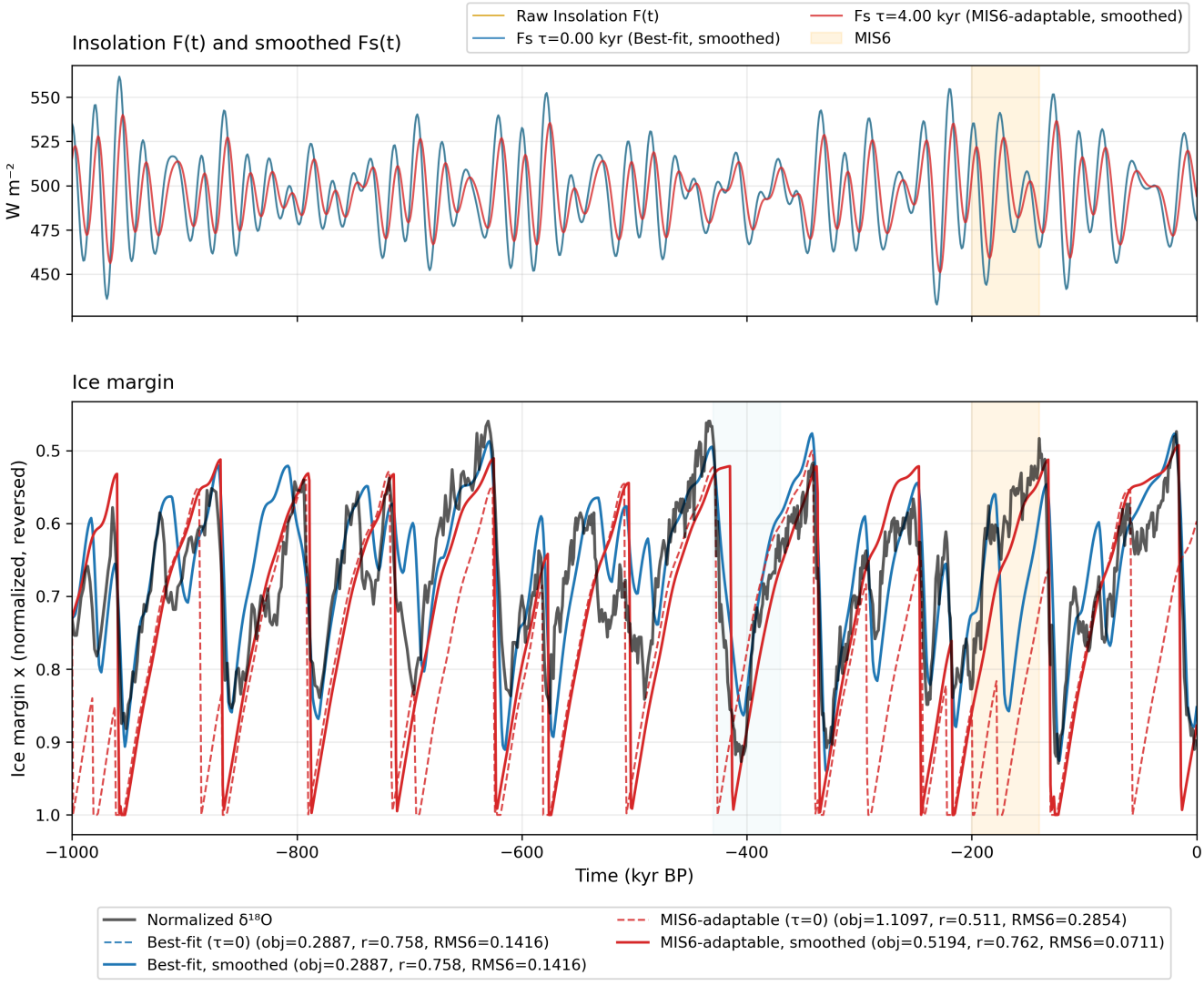

Figure 3. Top panel: June-21 65°N insolation forcing $F(t)$ (yellow) and its low-pass filtered variants $F_s(t)$ for the calibrated best-fit solution ($\tau = 0.00$ kyr, blue) and the MIS6-adaptable solution ($\tau = 4.00$ kyr, red). The low-pass differential equation $\mathrm{d}F_s/\mathrm{d}t = (F - F_s)/\tau$ is integrated on the same $\Delta t = 0.01$ kyr (10 yr) grid using an exact exponential update scheme. Bottom panel: comparison of simulated ice-margin trajectories without (dashed lines, $\tau = 0$) and with (solid lines, calibrated τ) low-pass forcing for both parameter sets against the normalized LR04 benthic δ^{18}O stack.

https://doi.org/10.5194/egusphere-2026-7112
Preprint. Discussion started: 25 November 2026
© Author(s) 2026. CC BY 4.0 License.



Figure 4. Glacial cycles during the last 2 million years. Top panel shows the insolation forcing, together with the insolation threshold F_0 in use in our model for the switching of the c values; the portions of the series where insolation exceeds such a limit are highlighted. The bottom panel shows in solid blue the δ^{18}O record, converted to x_{obs} according to Eq. 7, in solid green the results of our extended model with the best-fit parameters, in dashed orange the results from Paillard (1998), extended model; the vertical axis uses a reverse scale in order to show the trends in ice volume. A linear trend of 3 $\text{Wm}^{-2}\text{Myr}^{-1}$ for insolation was used for Paillard's model, as in Paillard (1998).

https://doi.org/10.5194/egusphere-2026-7112
Preprint. Discussion started: 25 November 2026
© Author(s) 2026. CC BY 4.0 License.

a control on the symmetry of the cycles (the lower it is, the more symmetric they are). Even when trying to rescale Paillard's linear trends on the [-2Myr,-0.8Myr] window only, such features remained (see Appendix B); moreover, we did not need to alter the insolation forcing, but only the model parameters.

The ensemble sampling demonstrates stability over its neighborhood: 428/500 (85.6%) of the members generated in the ellipsoidal neighborhood around the best-fit satisfy the strict 20% metric tolerance imposed simultaneously on $\mathcal{J}$, RMS, and r, with all compliant members accurately reproducing the late-Pleistocene glacial cycles (Fig. 5), although two eigenvalues out of ten are negative, meaning that H is not a squared basin.

A notable feature of this ensemble is the behavior of the interglacial-inertia coefficient D, which is physically constrained to $D \geq 0$ (Sect. 2). At $x = 1$ one has $u = 1$, and the term $d\,F$ can only matter if it keeps the net rate positive in the weak-insolation branch ($c = C_1$), i.e. if

$$\left(D + S\,(1 - x_H)^{-N} + C_1\,(1 - x_H)\right) F \;>\; B_1\,(1 - x_H)^{-N} + B_0, \tag{9}$$

so that the margin stays at $x = 1$ until F has decreased below the value at which the two sides are equal. For the best-fit set, taking F just below the threshold F_0 (normalised value 0.6501), this requires $D \gtrsim 0.02\,\mathrm{kyr}^{-1}$.

Because the calibrated best-fit value $D = 1.045 \times 10^{-4}\,\mathrm{kyr}^{-1}$ lies two orders of magnitude below this activation threshold, the exit from $x = 1$ is determined solely by the switch of c at F_0 rather than D. Moreover, the best-fit solution never reaches $x = 1$ (contrary to the MIS6-adaptable). Consequently, the $d\,F$ term remains inactive throughout the 1-Myr simulation, leaving 9 effective active parameters for this set ($\partial\mathcal{J}/\partial D \approx 0$). In Figure 5, the lower bound on D across the sampled ensemble is dictated by the physical non-negativity constraint $D \geq 0$ enforced during eigenvector bisection and LHS sampling, confirming that setting $D = 0$ yields a physically identical ice-margin trajectory and skill metrics.

For the MIS6-adaptable set $D = 0.01183\,\mathrm{kyr}^{-1}$ is close to, but still below, the corresponding threshold ($\approx 0.0124\,\mathrm{kyr}^{-1}$), so the dF term does not control the exit from $x = 1$ in this case either, but shifts it. We retain D in the general formulation as a possible inertia of the deglaciated state, but the present calibration does not constrain it.

5 Discussion

5.1 On the key role of transport

A central physical assumption underlying the present framework is that the meridional transport of heat and moisture is not independent of ice-sheet geometry, but instead responds dynamically to changes in the latitudinal extent of Northern Hemisphere ice sheets. In particular, we hypothesise that larger ice sheets enhance meridional energy transport toward their margins, thereby amplifying melt processes and potentially contributing to the rapidity of glacial terminations. This assumption contrasts with the classical view in which meridional transport is primarily controlled by insolation gradients alone, and it instead emphasises the role of large-scale atmospheric and oceanic circulation reorganisations induced by orographic forcing and by the presence of ice sheets.

https://doi.org/10.5194/egusphere-2026-7112
Preprint. Discussion started: 25 November 2026
© Author(s) 2026. CC BY 4.0 License.

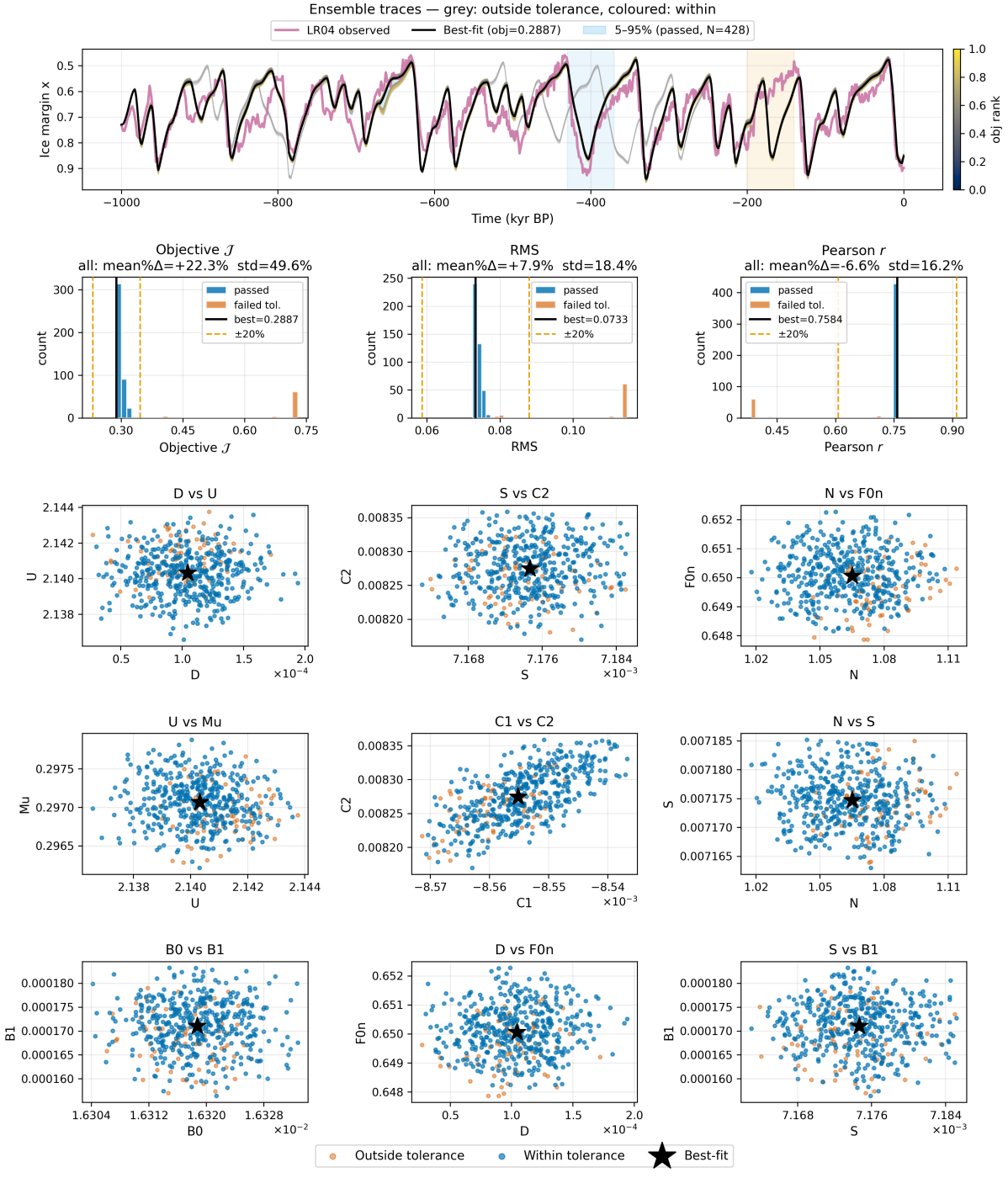

Figure 5. Sampling of the parameter space in the ellipsoidal neighborhood of the best-fit defined by the Hessian matrix. 500 ensemble members, ellipsoid axes calibrated by binary search to 20% metric tolerance. Members within tolerance: 428/500 (85.6%). Concerning D, the ellipsoid is truncated at the physical bound $D \geq 0$. Since $\mathcal{J}$ is insensitive to D in this range (Sect. 4.2), the extent of the ensemble along D reflects the eigenvector mixing and the numerical regularisation of a locally flat direction, not an empirical constraint on D.

https://doi.org/10.5194/egusphere-2026-7112
Preprint. Discussion started: 25 November 2026
© Author(s) 2026. CC BY 4.0 License.

Several lines of evidence support the idea that ice-sheet growth can substantially modify atmospheric circulation patterns. Idealised general circulation model experiments have shown that large Northern Hemisphere ice sheets are capable of inducing stationary wave responses that significantly reorganise mid-latitude circulation, thereby altering the distribution of heat transport across latitudes (Cook and Held, 1988). In particular, the presence of extensive topography associated with the Laurentide Ice Sheet can force quasi-stationary Rossby wave trains, which in turn modify storm-track activity and shift the pathways of transient eddies, leading to a systematic redistribution of meridional energy fluxes.

More recent modelling studies have further demonstrated that ice-sheet-induced orography can influence the position and intensity of storm tracks, with consequences for both atmospheric heat transport and regional climate sensitivity. For example, Liakka and Nilsson (2010) showed that the growth of Northern Hemisphere ice sheets affects the eddy-driven jet stream and storm-track dynamics, leading to non-trivial feedbacks between ice-sheet geometry and atmospheric circulation. In a similar context, coupled ice-sheet–climate experiments suggest that large ice sheets can reorganise stationary wave patterns and thereby modulate the meridional heat flux in a way that depends nonlinearly on ice-sheet size (Roe and Lindzen, 2001).

From a broader perspective, coupled climate–ice-sheet simulations have also highlighted the importance of atmosphere–ocean interactions in mediating the response of meridional heat transport to changes in ice-sheet extent. In particular, studies using intermediate-complexity Earth system models have shown that the presence of large ice sheets can alter both atmospheric and oceanic circulation patterns, leading to changes in heat transport that scale with ice-sheet volume and geometry (Ganopolski and Calov, 2011). Similarly, fully coupled simulations of glacial climates indicate that the Laurentide Ice Sheet in particular plays a dominant role in reorganising Northern Hemisphere circulation, with consequences for the global distribution of energy transport (Abe-Ouchi et al., 2013).

At the same time, a number of theoretical studies have emphasised that meridional heat transport in the climate system is strongly constrained by energy balance considerations and tends to increase with the meridional temperature gradient. In this framework, large ice sheets serve as powerful amplifiers of the zonal-mean equator-to-pole temperature gradient, primarily through their high surface albedo and high-latitude thermal cooling. Classical thermodynamic and energy-balance considerations establish that a steeper meridional temperature gradient enhances the total poleward atmospheric energy flux — driven predominantly by transient baroclinic eddies (Budyko, 1969; Stone, 1978; Pierrehumbert, 2010). As a result, expanding continental ice sheets naturally intensify the background atmospheric heat transport directed toward their southern ablation margin.

Although the discussion above has focused primarily on atmospheric pathways, a similar qualitative argument may apply to the oceanic component of meridional heat transport. The presence and growth of large ice sheets can modify large-scale wind stress patterns and buoyancy forcing at the ocean surface, thereby influencing the strength and geometry of the meridional overturning circulation. In particular, changes in the position and intensity of the westerly winds associated with ice-sheet-induced atmospheric circulation anomalies may affect Ekman transport and subpolar gyre dynamics, with consequences for northward ocean heat transport (Rahmstorf, 2002; Broecker, 1997). In addition, freshwater fluxes from ice-sheet margins can alter deep-water formation rates and stratification in the North Atlantic, thereby modulating the stability and variability of the Atlantic Meridional Overturning Circulation (Stommel, 1961; Stouffer et al., 2006). While these processes are not explicitly

https://doi.org/10.5194/egusphere-2026-7112
Preprint. Discussion started: 25 November 2026
© Author(s) 2026. CC BY 4.0 License.

represented in the present model, they suggest that the effective transport amplification associated with increasing ice-sheet extent may include both atmospheric and oceanic contributions.

Taken together, these processes highlight that the effective meridional heat transport is dynamically coupled to ice-sheet extent. In our model, this complex interplay is condensed into a single geometrically controlled transport term $(x-x_H)^{-N}$, which scales inversely with distance to the tropical boundary. We emphasize that specific regional pathways – such as topographically forced stationary Rossby waves that create localized cold eastern troughs (Cook and Held, 1988; Liakka and Nilsson, 2010) or meltwater-induced AMOC weakening that suppresses oceanic heat transport (Rahmstorf, 2002; Stouffer et al., 2006) – can exert local cooling or negative feedbacks on deglaciation. The term $(x-x_H)^{-N}$ is therefore not intended to represent localized wave patterns or ocean overturning dynamics directly, but rather the net, zonal-mean atmospheric energy transport driven by the intensified meridional temperature gradient, which we hypothesize to be predominantly ablative at the expanded southern ice margin.

5.2 Trigger versus sustain, and what u does and does not explain

The model distinguishes the *trigger* of a termination from the feedbacks that *sustain* it once under way. The sustaining feedbacks — ice-sheet structural instabilities, temperature-albedo and temperature-CO_2 feedbacks, the melt-elevation feedback — are bundled into the amplifier u (Eq. 5), and by construction $u = 1$ at the glacial minimum $x_{\min}$ itself, since the exponent $U(x - x_{\min})^{M_u}$ vanishes there. In this precise sense, the onset of a termination in the model does not require any of the feedbacks folded into u.

This separation is real but should not be overstated. For the calibrated exponent $M_u \approx 0.30 < 1$, the derivative of u with respect to $(x - x_{\min})$ diverges as $x \to x^+_{\min}$: the amplifier is inactive *exactly* at the reset point, but its marginal response is steep upon the very first displacement. The trigger and the onset of sustaining feedbacks are therefore formally distinct but temporally close together. Physically, this near-singular initial sensitivity may reflect fast, threshold-like margin processes – such as marine ice-margin ungrounding, ice-shelf calving (MISI/MICI), and the immediate loss of seasonal snow cover at the ablation edge – which react on sub-decadal timescales as soon as retreat begins. Slower Earth-system feedbacks bundled into u (such as atmospheric CO_2 outgassing, dust accumulation on exposed ice, and lithospheric bedrock rebound) take over as $x - x_{\min}$ grows, sustaining the multi-millennial trajectory of the termination.

It is important to distinguish two stages. The *reversal* of $\dot{x}$ (the onset of retreat) is governed by the trigger condition of Eq. (11), evaluated at $u = 1$: it occurs whenever the insolation exceeds F_{trig} (or $F \geq F_0$ for shallower glacials), and it also occurs at many local minima that produce only minor margin fluctuations, both in the model and in the proxy record (Fig. 2). Whether the reversal develops into a *committed termination* depends on what follows. The amplifier acts only on the insolation-dependent terms, so that once retreat has begun the rate is

$$\dot{x} = d\,F + u\left[S\,(x - x_H)^{-N} + c\,(x - x_H)\right] F - B_1\,(x - x_H)^{-N} - B_0, \tag{10}$$

with $u = \exp[U(x - x_{\min})^{M_u}]$ increasing with the cumulative retreat. Because $M_u \approx 0.10$–0.30 is small, u rises steeply for tiny retreats across the entire parameter range. For example, a minor retreat of $x - x_{\min} = 10^{-3}$ (about 0.2% of the glacial–

https://doi.org/10.5194/egusphere-2026-7112
Preprint. Discussion started: 25 November 2026
© Author(s) 2026. CC BY 4.0 License.

interglacial range) yields $(10^{-3})^{0.2971} \simeq 0.128$ and $u \simeq e^{2.140\times0.128} \simeq 1.32$ for the best-fit set. The retreat becomes self-sustaining if $(u-1)\left[S\,(x-x_H)^{-N} + c(x-x_H)\right] F$ keeps the net rate positive while F is still high enough; if instead F decreases before u has grown sufficiently, $\dot{x}$ changes sign again and $x_{\min}$ is reset, giving a minor oscillation. The trigger therefore sets when retreat can start, while the steep initial slope of u converts a small initial retreat into a runaway whose extent depends on the state of the system at the onset. As illustrated by the minor excursions throughout the simulated trajectories (Fig. 2), an initial sign reversal ($\dot{x} > 0$) does not automatically guarantee a committed deglaciation if insolation drops before u has built up sufficient momentum.

It is worth being explicit about what constitutes the trigger. At fixed x and with $u = 1$, the sign of $\mathrm{d}x/\mathrm{d}t$ is set by insolation: $SF(x-x_H)^{-N}$ grows linearly with F, whereas $B_1(x-x_H)^{-N}$ and B_0 do not depend on it. Retreat starts when F exceeds

$$F_{\mathrm{trig}}(x) = \frac{B_0 + B_1(x-x_H)^{-N}}{S(x-x_H)^{-N} + c(x-x_H)}, \tag{11}$$

which decreases as the ice sheet grows. With the reference parameters and $c = C_1$, $F_{\mathrm{trig}} < F_0$ only for $x - x_H \lesssim 0.274$, i.e. $x \lesssim 0.57$. For the deepest glacial states the trigger lies well below F_0 ($F_{\mathrm{trig}} \simeq 511\,\mathrm{W\,m^{-2}}$ at $x - x_H = 0.25$), and retreat begins through transport alone; closer to the limit it lies only a few $\mathrm{W\,m^{-2}}$ below F_0 (about 517.4 vs. 521.3 at $x - x_H = 0.265$), and for shallower glacials retreat starts when F crosses F_0 and c switches to C_2, which reinforces it. The trigger is therefore insolation itself, and the size of the ice sheet sets how much insolation is required for a termination.

A size-dependent insolation threshold is also found by Abe-Ouchi et al. (2013), who attribute it to isostatic depression: the bedrock beneath a large ice sheet is depressed and rebounds slowly, so the ice surface sits lower, and hence warmer by the lapse rate, than it would in equilibrium. This lowers the insolation (together with the CO_2 level) required to start a negative mass balance, and the delayed rebound then sustains the retreat, so isostasy acts at both stages. In our model the size dependence of the trigger is carried instead by transport geometry ($(x-x_H)^{-N}$), while isostasy is one of the sustaining feedbacks bundled in u, a memory of the recent history of the ice sheet that shapes how a retreat develops. The two mechanisms are physically different, geometric and atmospheric/oceanic in our case, elevation-based and lithospheric in theirs, and they are not mutually exclusive: both can operate in the real system, but a single state variable cannot tell them apart. What the present model shows is that transport geometry alone is sufficient to produce a size-dependent trigger.

It is worth remarking that the transport term $S\,F\,(x-x_H)^{-N}$ is not intended to represent atmospheric heat transport specifically. Both atmospheric and oceanic meridional transport are ultimately driven by the same equator-to-pole temperature gradient, and nothing in the present model distinguishes between them: S should be read as a lumped transport coefficient spanning both fluid systems, in the same spirit in which u (Sect. 2.3) lumps several physically distinct sustaining feedbacks into a single amplifier. This is a deliberate simplification rather than an oversight, but it is worth flagging explicitly, since the two transport channels differ enormously in response time — atmospheric reorganisation occurs over days, oceanic circulation over centuries — a distinction the single coefficient S cannot resolve.

This construction also resolves a difficulty faced by models that locate the termination trigger inside feedbacks such as ice-albedo or ice-sheet–CO_2 coupling. The core of a large ice sheet is thermally isolated enough that its temperature rarely approaches 0°C, so most proposed feedbacks can only act at the margin; it is then unclear how a bulk quantity such as total ice

https://doi.org/10.5194/egusphere-2026-7112
Preprint. Discussion started: 25 November 2026
© Author(s) 2026. CC BY 4.0 License.

volume, which Paillard (1998) identifies as the relevant state variable, could be communicated to the margin without an explicit transport pathway (unless margin-darkening is invoked). The geometric transport term introduced in Sect. 2.4, $SF(x-x_H)^{-N}$, is precisely this pathway: it lets the margin's response depend on the ice sheet's overall extent (through x) without requiring the ice-sheet interior itself to respond to insolation or albedo forcing. Volume-dependence is thus carried by geometry rather than by the assumption of a spatially uniform, feedback-sensitive ice sheet.

Over the last 1 Myr the calibrated model has 22 reversals of $\mathrm{d}x/\mathrm{d}t$ (glaciation $\rightarrow$ retreat). Of these, 15 develop into committed terminations (retreat amplitude ≥ 0.2 in x) and 7 are minor oscillations; no retreat is shorter than 0.5 kyr, so there is no numerical chattering. Nine of the 15 committed terminations start with $F < F_0$ ($c = C_1$, transport alone) and six with $F \geq F_0$, where the switch of c also contributes to the trigger.

5.3 Reconciling the albedo and CO_2 feedbacks with Sect. 2.3

Because u is inactive at the trigger, the discussion above lets us be more precise about the role of the individual feedbacks listed in Sect. 2.3 as candidate contributors to u — dust exposure, lack of fresh snow, the melt-elevation feedback, and the temperature-CO_2 feedback — without contradicting the objections raised against several of them as *triggers*. All of these mechanisms are retained here only as possible *sustaining* amplifiers, active after retreat has begun; none is required, or assumed, to initiate it. This statement concerns the sign reversal of $\dot{x}$. The same feedbacks, through u, are however what turns a reversal into a committed termination, as discussed in Sect. 5.2.

Dust-driven albedo lowering is a natural candidate for such a sustaining role, but is an ambiguous candidate for the trigger itself. Terminations begin when insolation is high, which warms the ice-free regions that supply the ice sheet's moisture. The resulting increase in precipitation delivers fresh snow to the margin, raising its albedo faster than dust deposition can lower it, at least while the accumulation zone is still intact. Only once ablation has substantially exposed older, debris-laden ice — i.e., after retreat is already under way — does dust plausibly dominate the local albedo balance. This is consistent with treating the dust-albedo mechanism as part of u rather than as part of the trigger term.

The temperature-CO_2 feedback raises a similar issue, though the observational picture is more contested than is sometimes assumed. Two independent ice-core-based estimates of the relative phasing of Antarctic temperature and atmospheric CO_2 across deglaciations (Fischer et al., 1999; Monnin et al., 2001) suggested that Antarctic warming led the CO_2 rise by several centuries; a revised chronology based on nitrogen-isotope constraints on gas-ice age offsets found no significant asynchrony between the two at the four abrupt transitions examined during the last deglaciation (Parrenin et al., 2013), while a global (rather than Antarctic-only) temperature reconstruction found that global temperature generally lags, rather than leads, CO_2 during the same interval (Shakun et al., 2012). These are two distinct comparisons — regional Antarctic temperature vs. CO_2, and global temperature vs. CO_2 — and do not straightforwardly agree with one another on lead-lag order, which cautions against treating the phasing as settled. What the comparisons do agree on is that CO_2 is not obviously running *far* ahead of high-latitude warming at the onset of a termination, which is enough to argue against a CO_2-driven *trigger*; it says nothing against a CO_2 feedback contributing to the amplification of a termination once temperature has begun to rise, which is the only role we assign it here, via u.

https://doi.org/10.5194/egusphere-2026-7112
Preprint. Discussion started: 25 November 2026
© Author(s) 2026. CC BY 4.0 License.

5.4 On the ambiguities and potentials of our model

Eq. 3 is a simple ODE that only needs the normalized insolation F as a forcing, it provides realistic and robust results, it introduces a new possible interpretation of deglaciation onsets and of the 100 kyr cyclicity during the last 800 kyrs and its terms are physically interpretable.

However, it also has its limitations. It makes several assumptions, some of which are reasonable: the direct proportionality of the southern margin of the ice sheet x to the ice volume, the bulk of the ice sheet not being affected by ablation. Some others which are daring: the inclusion of the insolation itself as a proxy for temperature in the local ablation term, the direct proportionality of all transport to temperature gradients, the independence of snowfall on temperature to the first order with respect to the dependence of ablation on temperature. Finally, it does not distinguish atmospheric and oceanic transport, nor does it distinguish the different feedbacks that amplify the terminations through u. The reason behind all these simplifications is to keep the model as simple as possible, although physically motivated. They can be overcome by increasing model complexity: coupling an energy balance equation at the margin avoids using insolation as a proxy for temperature; coupling an albedo evolution scheme that explicitly depends on meltwater and dust avoids the obscurity of coefficient c, separating ocean from atmosphere implies distinguishing the relative kinds of transport, etc.. This would for sure weaken the main purpose of this work: to provide a simple explanation of the mechanism behind glacial cycles in the last part of the Pleistocene.

Moreover, the simplicity of our model makes it easy to couple it with other conceptual models in the climate system, e.g. Stommel's model for AMOC (Stommel, 1961), which we reserve to implement in a future work.

The 2 Ma extension of the model also needs some discussion. First, the fact that U is one of the time-dependent parameters could mean that the nature of feedbacks is what actually changes between the two parts of the Pleistocene, due to some external factor: for example, the removal of regoliths could favor the isostasy feedback, or an enhanced CO_2 cycle could favor the temperature-CO_2 feedback. The other parameter that depends on time, x_H, is coherent to Paillard's idea of a maximum-volume increase with time, but it cannot be physically interpreted as a shrinking of the Hadley cell only: an initial Hadley cell covering 54% of latitudes (Table 1) would be unrealistic; however, the reason for its shifting is that it acts as a moving lower asymptote on x: it shifts the $x = x_H$ transport singularity poleward across the mid-latitudes prior to 800 ka. Since for $x < 1$ every term of Eq. (3) depends on x only through $(x - x_H)$, a larger x_H translates the whole dynamics towards $x = 1$: the same trigger distance $(x - x_H)$ (Sect. 5.2) is reached at larger x, so that glacial minima are less deep and the range available for the margin, $1 - x_{\mathrm{trig}}$, is reduced. At $x = 1$ the transport terms are also stronger, because $1 - x_H$ is smaller ($(x - x_H)^{-N} \simeq 2.29$ for $x_H = 0.54$ against 1.46 for $x_H = 0.30$, with $N = 1.065$). The concurrent reduction of U weakens the runaway driven by u and makes the cycles more symmetric, so that the two drifts together produce the smaller and more symmetric early-Pleistocene oscillations. Here x_H is thus an effective parameter, which probably embeds other mechanisms, such as the tectonic configuration of the continents or the average global CO_2 concentration.

A formal comparison between a gradual and an abrupt change of U and x_H, in the spirit of Legrain et al. (2023), would be required to turn the demonstration of Sect. 2.5 into a test, and is left for future work.

https://doi.org/10.5194/egusphere-2026-7112
Preprint. Discussion started: 25 November 2026
© Author(s) 2026. CC BY 4.0 License.

6 Conclusions

We have presented a conceptual model of Late Pleistocene glacial cycles in which a single ordinary differential equation governs the latitude of the Northern Hemisphere ice-sheet margin under summer insolation forcing. Its central ingredient is a geometry-dependent meridional transport of heat and moisture, which grows as the margin approaches the boundary of the Hadley cell, combined with a history-dependent amplifier that accounts for the feedbacks acting during retreat. In contrast to previous threshold models, rapid deglaciations arise from the evolution of the governing equation rather than being imposed through prescribed state transitions. The model still contains piecewise functions governed by thresholds, but each has an explicit physical interpretation, and for the deepest glacial states they appear to act in sustaining the deglaciation rather than in triggering it.

Calibrated on the LR04 benthic δ^{18}O stack, the model reproduces the main features of the last million years: the sawtooth shape of the cycles, their asymmetry between slow growth and rapid collapse, their irregular spacing, and most of the major terminations, with a skill comparable to a Paillard model recalibrated on the same target, and better than its published version (Paillard, 1998) in some metrics. Known misfits remain, notably MIS6, where a termination occurs that is absent in the record unless the forcing is smoothed, and a few intermediate glacial maxima. Letting two parameters, U and x_H, drift linearly before the Mid-Pleistocene Transition is enough to reproduce the lower amplitude and shorter period of the early Pleistocene. Since the values of this drift were chosen by hand and checked on the same record, we regard the 2 Myr result as a demonstration that a monotonic change of two parameters suffices, not as an estimate of them.

The model suggests a division of roles. The trigger of a termination is insolation, and the size of the ice sheet sets how much insolation is needed: through the transport term, which grows as the margin moves equatorward, deep glacial states tend to begin their retreat at insolation below F_0, before the albedo switch c changes value from C_1 to C_2 in response to insolation. For these states the switches do not trigger the termination; the switch in c and the amplifier u reinforce and sustain it. This holds only for the larger glaciations: shallower ones, where the transport term is weaker, require c to switch as well, so that in these cases the threshold also contributes to the trigger. Once retreat has begun, the amplifier u, which stands for ice-sheet instabilities, albedo lowering, melt–elevation and CO_2 feedbacks and, in a broad sense, isostatic depression, makes it run away, so that the speed and extent of a termination depend continuously on the state of the system at the onset. In this sense the volume threshold of Paillard (1998) is replaced by a continuous dependence on margin geometry and on cumulative retreat. Each switch is tied to an identifiable process, but their values are calibrated, not derived. A local expansion shows that, between switches, the equation has the structure of the relaxation equation of Paillard (1998), with coefficients that depend on the state and on the history, and with an effective relaxation rate that becomes unbounded at the onset of a retreat.

The model rests on simplifications that the data cannot test by themselves. Insolation stands in for temperature; transport by atmosphere and ocean is lumped into a single coefficient; accumulation is assumed independent of insolation (at the scale of the ice-sheet interior, i.e. in the transport term; a local sub-threshold dependence is contained in C_1), so that the calibrated coefficient of the heat-transport term is a net sensitivity; and the feedbacks included in u are not separated. Parameters were obtained from a search that found a good local optimum and not a demonstrated global one, and a second, structurally different

https://doi.org/10.5194/egusphere-2026-7112
Preprint. Discussion started: 25 November 2026
© Author(s) 2026. CC BY 4.0 License.

solution exists, with larger error on the full record but better behaviour at MIS6 under smoothed forcing. Isostasy, which Abe-Ouchi et al. (2013) propose as the origin of a size-dependent threshold, cannot be distinguished from the transport geometry with a single state variable; our result is that the latter is sufficient, not that it is the only possibility.

These assumptions lead to testable statements. The model predicts that the transport toward the ice margin increases as the margin extends equatorward, approximately as an inverse power of its distance from the Hadley boundary, and that this increase is what makes large ice sheets more sensitive to insolation. This can be examined in intermediate complexity models and in coupled ice-sheet–climate simulations by diagnosing the meridional transport as a function of ice extent. Further steps are a deeper analytical study of the equation, the separation of atmospheric and oceanic transport, the coupling with simplified energy-balance and carbon-cycle equations, and the replacement of the switches by explicit processes. If the mechanism is confirmed, the present formulation would provide a minimal and physically interpretable link between orbital forcing, meridional transport and nonlinear ice-sheet dynamics in the Quaternary glacial cycles.

Code and data availability. The source code of the 1-ODE conceptual model, including calibration scripts, sensitivity analysis, and figure generation routines, is open-source under the MIT License. Version 1.0.2 of the code used in this study is permanently archived on Zenodo at https://doi.org/10.5281/zenodo.24165064 (Maiero et al., 2026) and is actively maintained on GitHub at https://github.com/emaiero-jpg/transport-model-glaciations.

https://doi.org/10.5194/egusphere-2026-7112
Preprint. Discussion started: 25 November 2026
© Author(s) 2026. CC BY 4.0 License.

Appendix A: Numerical information

Numerical details about the ensemble bounds for the calibration (Table A1; see Sect. 3.3) and for the numerical stability with respect to the timestep (Table A2; see Sect. 3.1), and the top 10 calibrated parameter sets by ascending cost function $\mathcal{J}$ (Table A3; see Sect. 3.3).

Table A1. Parameter bounds used for the Latin hypercube sampling (Stage 1 of the calibration). The constraints $C_1 < C_2$ and $D \geq 0$ were imposed on the objective.

Parameter	Lower bound	Upper bound
D [kyr^{-1}]	0.0	0.20
U	1.0	15.0
S [kyr^{-1}]	$5 \cdot 10^{-4}$	0.015
C_1 [kyr^{-1}]	-0.020	0.010
C_2 [kyr^{-1}]	-0.010	0.060
B_0 [kyr^{-1}]	0.002	0.030
B_1 [kyr^{-1}]	10^{-5}	0.003
N	1.0	5.0
F_0 (normalised)	0.25	0.85
M_u	0.05	5.0

Table A2. Sensitivity of the results to the length of the time step Δt [kyr].

	Best-fit			MIS6-adaptable		
Δt [kyr]	$\mathcal{J}$	RMS	r	$\mathcal{J}$	RMS	r
0.1	0.3057	0.0740	0.7506	1.1060	0.1645	0.5157
0.01	0.2887	0.0733	0.7584	1.1097	0.1649	0.5111
0.001	0.2884	0.0733	0.7588	1.1104	0.1651	0.5107
0.0001	0.2884	0.0733	0.7589	1.1105	0.1651	0.5107

https://doi.org/10.5194/egusphere-2026-7112
Preprint. Discussion started: 25 November 2026
© Author(s) 2026. CC BY 4.0 License.

Table A3. Best-fit parameters by ascending cost function $\mathcal{J}$, which is reported on the first row. Rows from the second to the second-to-last one report the parameters, the last one is the dimensional threshold in insolation.

Parameter	**Rank 1**	**Rank 2**	**Rank 3**	**Rank 4**	**Rank 5**	**Rank 6**	**Rank 7**	**Rank 8**	**Rank 9**	**Rank 10**
$\mathcal{J}$	0.28865	0.29112	0.29120	0.29162	0.29194	0.29254	0.29313	0.29329	0.29335	0.29544
$D \times 10^4$ [kyr^{-1}]	1.0454	1.0662	1.3290	1.0300	0.8343	1.3851	1.2491	1.4131	1.2673	1.0312
U	2.1403	1.9330	1.8460	2.0053	1.9560	2.0706	1.9386	1.8616	1.7714	1.8332
$S \times 10^3$ [kyr^{-1}]	7.1747	6.3467	7.2436	6.9137	7.8703	5.6636	5.6571	6.3441	7.5005	6.2163
$C_1 \times 10^3$ [kyr^{-1}]	-8.5552	-6.1645	-5.8955	-6.1292	-7.3625	-7.4435	-4.9484	-5.4939	-4.6670	-5.8237
$C_2 \times 10^3$ [kyr^{-1}]	8.2745	8.6799	8.3253	9.5585	8.3502	7.6836	8.9577	8.1820	9.5483	8.6446
$B_0 \times 10^2$ [kyr^{-1}]	1.6319	1.6447	1.7077	1.6475	1.7065	1.5478	1.6070	1.6528	1.8032	1.6582
$B_1 \times 10^4$ [kyr^{-1}]	1.7102	1.6847	2.2975	1.8613	2.2212	1.8184	1.6791	2.1503	1.4752	1.7385
N	1.0652	1.1457	1.0697	1.0604	1.0144	1.1976	1.2138	1.1434	1.0760	1.1582
F_0	0.6501	0.6216	0.6221	0.6163	0.6572	0.6219	0.6219	0.6214	0.6216	0.6225
M_u	0.2971	0.2407	0.2329	0.2707	0.2643	0.2467	0.2325	0.2156	0.2362	0.2064
F_0^{dim} (W m^{-2})	521.31	516.95	517.03	516.15	522.42	516.99	516.99	516.92	516.95	517.09

https://doi.org/10.5194/egusphere-2026-7112
Preprint. Discussion started: 25 November 2026
© Author(s) 2026. CC BY 4.0 License.



Appendix B: Recalibration of Paillard's model

We recalibrated Paillard's model with the same recipe as in Sect. 3.3 against LR04 (but with 1000 starting points and Nelder-Mead on the 20 best results), finding an improvement of about 19% in RMS with respect to the original parameters over the last 1Ma (at the expense of a lower correlation, r from 0.8039 to 0.7685, since $\mathcal{J}$ penalises amplitude errors, not phase): with $\tau_i = 14.50$ kyr, $\tau_g = 37.36$ kyr, $\tau_G = 47.84$ kyr, $V_R = 0.849$, $\tau_F = 36.92$ kyr, the RMS (including MIS6 and MIS11) amounts to 0.0747 and $r = 0.7685$ (Fig. B1). The parameters were bounded at [2.0,30.0] kyr, [15.0,90.0] kyr, [15.0,90.0] kyr, [0.5,1.5] and [10.0, 50.0] kyr for τ_i, τ_g, τ_G, V_R, τ_F respectively. The insolation and volume thresholds were kept as in the original model.

The switching thresholds (i_0, i_1, V_0) were intentionally retained at their original published values (Paillard, 1998) to evaluate how adjusting only the internal timescale and relaxation parameters improves the fit to LR04 while preserving the model's original state-transition structure.

Concerning the 2Ma extension, we tried to use the original Paillard's parameters, the original Paillard's parameters but with the linear trends on V_R and on insolation only from -2 Myr to -0.8 Myr (with the same starting values of the parameters at -2 Myr as before, but with modern values reached at -0.8 Myr), the recalibrated parameters with the linear trends on V_R and on insolation only from -2 Myr to -0.8 Myr, finding respectively RMS = 0.1642 and $r = 0.4559$, RMS = 0.1331 and $r = 0.5943$, RMS = 0.0949 and $r = 0.6451$ (Fig. B2).

https://doi.org/10.5194/egusphere-2026-7112
Preprint. Discussion started: 25 November 2026
© Author(s) 2026. CC BY 4.0 License.

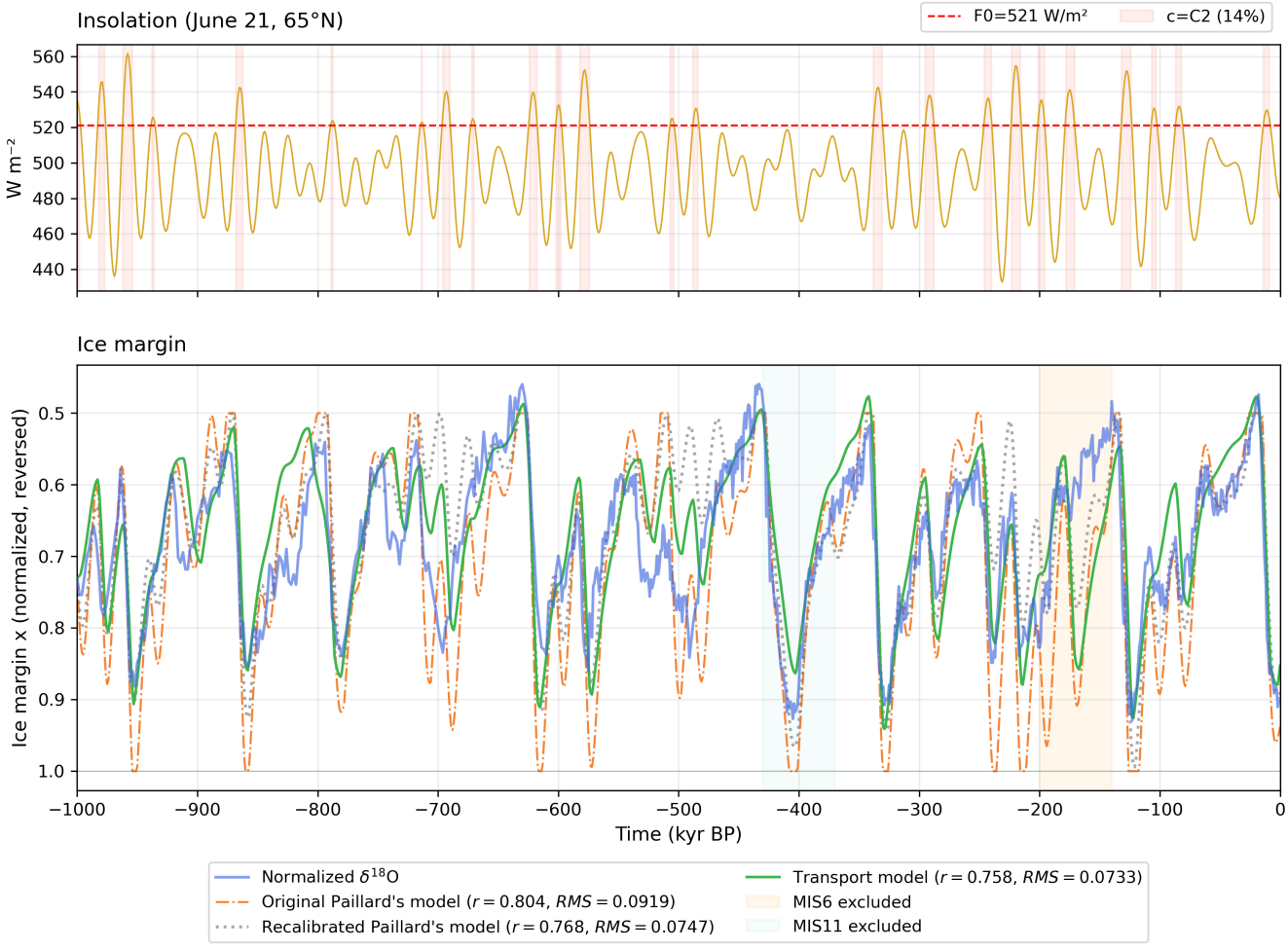

Figure B1. Glacial cycles during the last million years. Top panel shows the insolation forcing, together with the insolation threshold F_0 in use in our model for the switching of the c values; the portions of the series where insolation exceeds such a limit are highlighted. The bottom panel shows in solid blue the δ^{18}O record, converted to x_{obs} according to Eq. 7, in solid green the results of our model with the best-fit parameters, in dashed orange the results from Paillard (1998), in dotted grey the results from the recalibrated Paillard's model; the vertical axis uses a reverse scale in order to show the trends in ice volume.

https://doi.org/10.5194/egusphere-2026-7112
Preprint. Discussion started: 25 November 2026
© Author(s) 2026. CC BY 4.0 License.

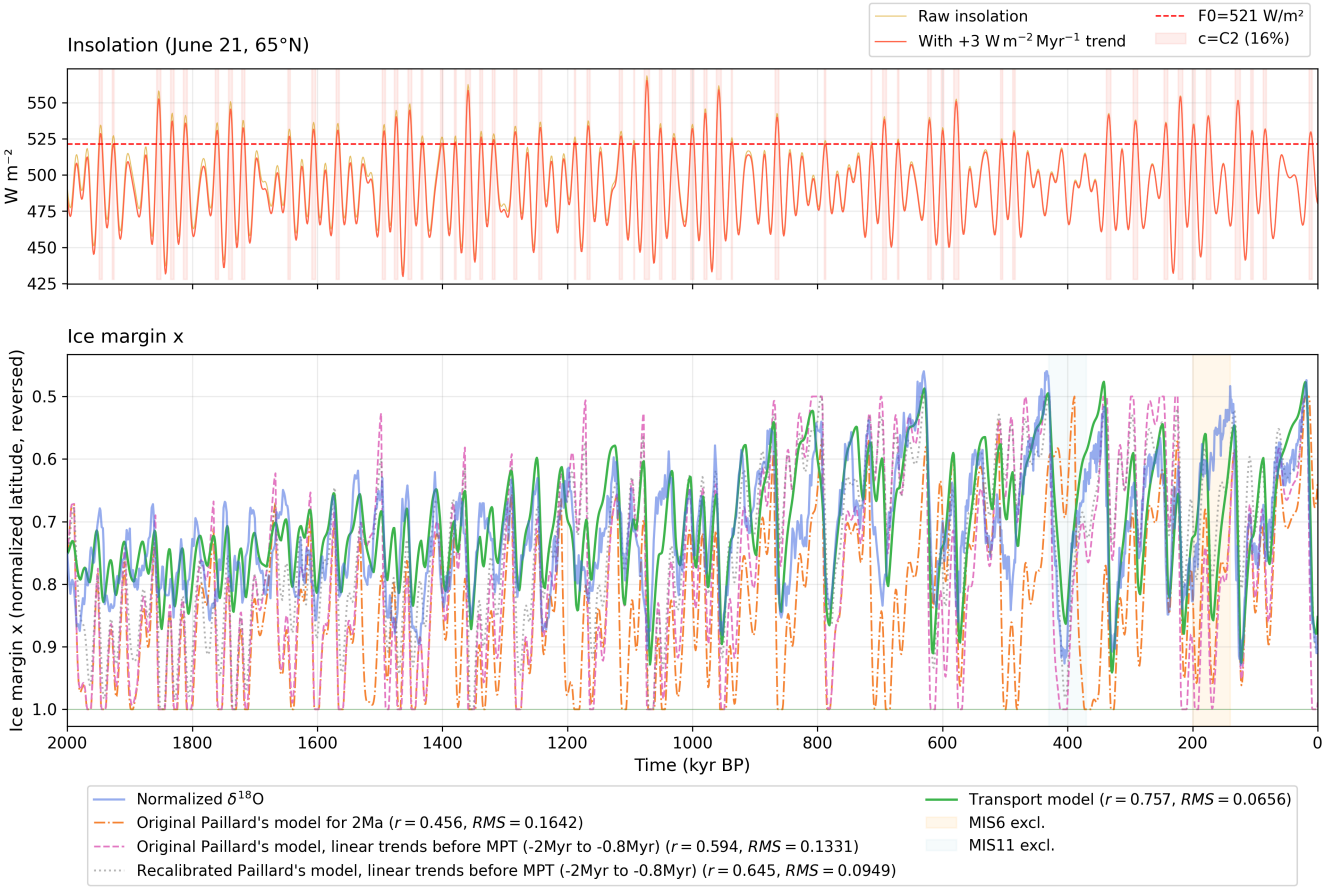

Figure B2. Glacial cycles during the last 2 million years. Top panel shows the insolation forcing, together with the insolation threshold F_0 in use in our model for the switching of the c values; the portions of the series where insolation exceeds such a limit are highlighted. The bottom panel shows in solid blue the δ^{18}O record, converted to x_{obs} according to Eq. 7, in solid green the results of our extended model with the best-fit parameters, in dashed orange the results from Paillard (1998) extended model, in dashed pink the results obtained with the original parameters from Paillard (1998) extended model but with the linear trends limited to [-2.0,-0.8]Myr, in dotted grey the results from the recalibrated Paillard's model with the linear trends limited to [-2.0,-0.8]Myr; the vertical axis uses a reverse scale in order to show the trends in ice volume. A linear trend of 3 $\text{Wm}^{-2}\text{Myr}^{-1}$ for insolation was used for Paillard's original model, as in Paillard (1998), and of 5 $\text{Wm}^{-2}\text{Myr}^{-1}$ over [-2.0,-0.8]Myr for the other two versions of Paillard's model.

https://doi.org/10.5194/egusphere-2026-7112
Preprint. Discussion started: 25 November 2026
© Author(s) 2026. CC BY 4.0 License.

Appendix C: Model performance against sea-level data

Because sea level is high when ice volume is low, whereas δ^{18}O increases with ice volume, the Spratt and Lisiecki (2025) sea-level stack (first principal component of the five-record stack, 0–798 ka) is sign-adjusted and linearly mapped onto the same state range spanned by the transformed LR04 δ^{18}O target over the overlapping 0–798 ka window. Defining $p(t) \equiv -\mathrm{SL}(t)$,

$$x_{\mathrm{obs}}(t) = \mathrm{clip}\left\{ q_{99} - (q_{99} - q_1)\,\frac{p(t) - p_1}{p_{99} - p_1},\, 0,\, 1 \right\}, \qquad p_1 = -\mathrm{SL}_{99}, \quad p_{99} = -\mathrm{SL}_1, \tag{C1}$$

where $\mathrm{SL}_1 = -123.80$ m and $\mathrm{SL}_{99} = +12.47$ m are the 1st and 99th percentiles of the native-resolution sea-level stack over 0–798 ka before interpolation onto the Δt model grid, and $q_1 = 0.468$, $q_{99} = 0.910$ are the 1st and 99th percentiles of the transformed LR04 series $x_{\mathrm{LR04}}(t)$ over the same 0–798 ka window (where $x_{\mathrm{LR04}} = 1$ corresponds to the 1st percentile of the full LR04 stack and $x_{\mathrm{LR04}} = 0.5$ to its 99th percentile). Equivalently, $x_{\mathrm{obs}} = q_1 + (q_{99} - q_1)(\mathrm{SL} - \mathrm{SL}_1)/(\mathrm{SL}_{99} - \mathrm{SL}_1)$, so that $x_{\mathrm{obs}} = q_{99}$ at SL_{99} (interglacial state) and $x_{\mathrm{obs}} = q_1$ at SL_1 (glacial maximum), ensuring a like-for-like RMS comparison without re-calibrating the model parameters.

Percentiles rather than extrema are used to make the scaling robust to isolated extreme values of the stack: roughly 1% of the samples at each tail fall outside $[q_1, q_{99}]$ without being truncated, while the $[0, 1]$ clipping bounds act only as numerical safeguards. Because the full LR04 transformation maps the 1st–99th percentile range onto $[0.5, 1]$—leaving the interval $(x_H, 0.5)$ free above the lower boundary $x_H = 0.3$ (chosen to approximately coincide with the margin of the Hadley cell)—this rescaling places the sea-level proxy in the exact same region of the model state space as the LR04 target used for calibration.

https://doi.org/10.5194/egusphere-2026-7112
Preprint. Discussion started: 25 November 2026
© Author(s) 2026. CC BY 4.0 License.

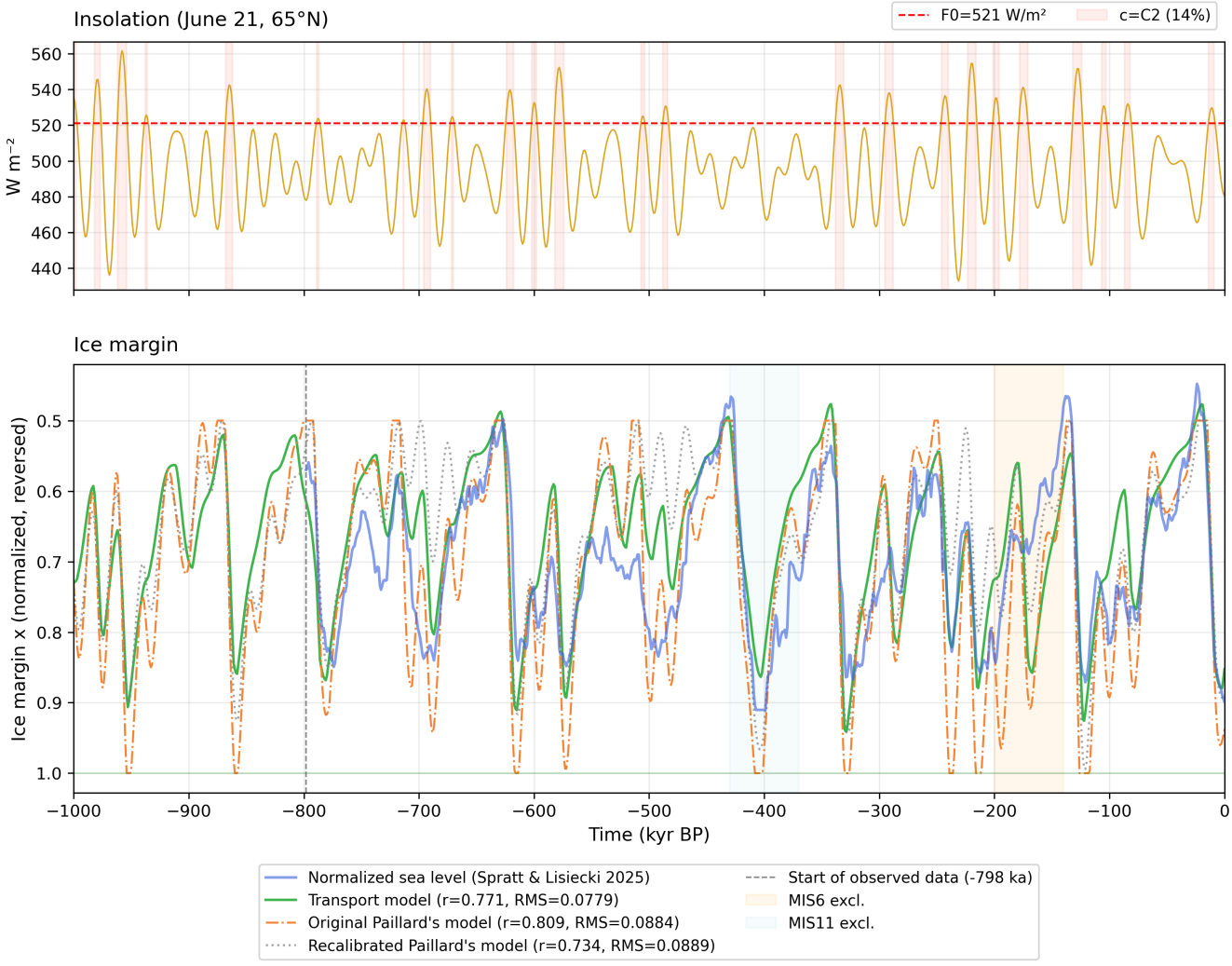

Figure C1. Glacial cycles during the last million years. Top panel shows the insolation forcing, together with the insolation threshold F_0 in use in our model for the switching of the c values; the portions of the series where insolation exceeds such a limit are highlighted. The bottom panel shows in solid blue the sea-level reconstruction from Spratt and Lisiecki (2025), converted to x_{obs} according to Eq. C1, in solid green the results of our model with the best-fit parameters, in dashed orange the results from Paillard (1998), in dotted gray the results from the recalibrated Paillard's model; the vertical axis uses a reverse scale in order to show the trends in ice volume. The models started at -1 Myr for the sake of comparison with Fig. 2, but the sea level data start at -798 kyr, after the Mid-Pleistocene transition. The starting point of simulations is the same as in Fig. 2, namely the value of the transformed δ^{18}O at -1Myr.

https://doi.org/10.5194/egusphere-2026-7112
Preprint. Discussion started: 25 November 2026
© Author(s) 2026. CC BY 4.0 License.

Appendix D: Analytical Relationship to the Paillard (1998) Model

First, let us begin by replacing V in Eq. 1 with $V = H(1-x)$ and $V_R = H(1-x_R)$, where H is an effective ice thickness. This leads to:

$$\frac{\mathrm{d}x}{\mathrm{d}t} = \frac{F}{H\tau_F} - \frac{x - x_R}{\tau_R} \tag{D1}$$

Now, let us Taylor-expand to the first order in x all terms that depend on x in Eq. 3 around a given x_0:

$$\begin{aligned}\frac{dx}{dt} =& d \cdot F + u(x_0, w(\dot{x}_0), history)[1 + h(x_0, history) w(\dot{x}_0)(x - x_0)] \cdot \\ & \cdot \left[S\,F\,(x_0 - x_H)^{-N} - N\,S\,F\,(x_0 - x_H)^{-N-1}\,(x - x_0) + c\,F\,(x_0 - x_H) + c\,F\,(x - x_0)\right] \\ & - B_1\,(x_0 - x_H)^{-N} + N\,B_1\,(x_0 - x_H)^{-N-1}\,(x - x_0) - B_0,\end{aligned} \tag{D2}$$

where $w(\dot{x}) = 1$ if $\dot{x} > 0$, $w(\dot{x}) = 0$ otherwise and h is a function of x_0 and the history. The expansion of u in Eq. (D2) applies on the retreat branch at interior points, $x_0 > x_{\min}$ and $\dot{x}_0 > 0$, where $h(x_0, history) = UM_u(x_0 - x_{\min})^{M_u - 1}$ is finite; during glaciation $u \equiv 1$ and no expansion of u is needed. At the onset of a retreat, $x_0 = x_{\min}$, the expansion does not exist for the calibrated exponent $M_u < 1$: u is continuous there but only Hölder-continuous, $u \simeq 1 + U(x - x_0)^{M_u}$, and its slope diverges. The effective relaxation rate τ_R^{-1} identified above is therefore finite on the retreat branch and unbounded at its start. This is the point at which the present model departs from the finite-gain relaxation of Paillard (1998), where the $\mathbf{G} \to \mathbf{i}$ transition is a jump between two linear regimes: here the system is maximally sensitive to the first retreat, and the local equivalence established below holds only from the second step of a termination on. Eq. D2 becomes, by rearranging the terms and neglecting second-order terms:

$$\begin{aligned}\frac{dx}{dt} =& \left[d(x_0) + u(x_0, w(\dot{x}_0), history)\,S\,(x_0 - x_H)^{-N} + u(x_0, w(\dot{x}_0), history)\,c\,(x_0 - x_H)\right] F \\ & + \left[u(x_0, w(\dot{x}_0), history)\,S\,F\,(x_0 - x_H)^{-N} h(x_0, history) w(\dot{x}_0)\right. \\ & + u(x_0, w(\dot{x}_0), history) cF(x_0 - x_H) h(x_0, history) w(\dot{x}_0) - u(x_0, w(\dot{x}_0), history) NSF(x_0 - x_H)^{-N-1} \\ & \left. + u(x_0, w(\dot{x}_0), history)\,c\,F + N\,B_1 (x_0 - x_H)^{-N-1}\right](x - x_0) \\ & - B_1\,(x_0 - x_H)^{-N} - B_0\end{aligned} \tag{D3}$$

We note that in an expansion of F around $F(t_0)$ (the value F takes at time t_0, when $x(t_0) = x_0$) the higher-order terms produced in the second element of Eq. D3 are second order terms of the type $(F - F(t_0))(x - x_0)$, so we can replace F with

https://doi.org/10.5194/egusphere-2026-7112
Preprint. Discussion started: 25 November 2026
© Author(s) 2026. CC BY 4.0 License.

$F(t_0)$ within this term (similar considerations hold for c and for u in both the first and the second squared brackets):

$$\begin{aligned}\frac{dx}{dt} &= \big[d(x_0) + u(x_0, w(\dot{x}_0), history)\, S\,(x_0 - x_H)^{-N} + u(x_0, w(\dot{x}_0), history)\, c(F(t_0))\,(x_0 - x_H)\big] F \\ &+ \big[u(x_0, w(\dot{x}_0), history)\, S\, F(t_0)\,(x_0 - x_H)^{-N} h(x_0, history) w(\dot{x}_0) \\ &\quad + u(x_0, w(\dot{x}_0), history) c(F(t_0)) F(t_0)(x_0 - x_H) h(x_0, history) w(\dot{x}_0) - u(x_0, w(\dot{x}_0), history) N S F(t_0)(x_0 - x_H)^{-N-1} \\ &\quad + u(x_0, w(\dot{x}_0), history)\, c(F(t_0))\, F(t_0) + N\, B_1 (x_0 - x_H)^{-N-1}\big] x \\ &- \big[u(x_0, w(\dot{x}_0), history) S F(t_0)(x_0 - x_H)^{-N} h(x_0, history) w(\dot{x}_0) \\ &\quad + u(x_0, w(\dot{x}_0), history) c(F(t_0)) F(t_0)(x_0 - x_H) h(x_0, history) w(\dot{x}_0) - u(x_0, w(\dot{x}_0), history) N S F(t_0)(x_0 - x_H)^{-N-1} \\ &\quad + u(x_0, w(\dot{x}_0), history)\, c(F(t_0))\, F(t_0) + N\, B_1 (x_0 - x_H)^{-N-1}\big] x_0 \\ &- B_1\,(x_0 - x_H)^{-N} - B_0 \end{aligned} \tag{D4}$$

This has the same structure of Eq. D1 if we identify the term in squared brackets that multiplies F with $H^{-1}\tau_F^{-1}$, the term in squared brackets multiplying x with $-\tau_R^{-1}$ and what is left with $x_R\tau_R^{-1}$. For Paillard (1998), τ_R depends on the state (**G**, **g** or **i**), which for us is clear for its explicit expression, although we also introduce a dependence on the sign of the derivative of x and on the last maximum volume through u (and w); x_R depends on the volume only for Paillard, whereas here $x_R = x_0 + [B_1(x_0 - x_H)^{-N} + B_0]/\mathcal{B}$ depends strongly on insolation and u through $\mathcal{B} = \partial\dot{x}/\partial x$, diverging and changing sign as $\mathcal{B}$ crosses zero between stable relaxation and runaway retreat; F does not have a varying response time for Paillard, but it has a varying one for us. The expansion holds within a branch (constant c, d and retreat mode), so it is not applied at turning points, which are the boundaries between branches. At a local minimum ($x_0 = x_{\min}$) the two branches agree, since $u = 1$ on both sides, and $\mathrm{d}x/\mathrm{d}t$ is continuous; its derivative with respect to x is finite on the glaciation side and, for $M_u < 1$, unbounded on the retreat side. At a local maximum with $x_0 > x_{\min}$, u jumps from $\exp[U(x_0 - x_{\min})^{M_u}]$ to 1 and $\mathrm{d}x/\mathrm{d}t$ is discontinuous by $-(u-1)\left[SF(x_0 - x_H)^{-N} + cF(x_0 - x_H)\right]$, which is negative whenever the bracket is positive (as it is for $c = C_2$ and, for the calibrated parameters, also for $c = C_1$ at the values of x_0 we checked): for the calibrated parameters, $x(t)$ has a corner, and the end of a retreat is followed by an abrupt onset of glaciation. Note that in the interior domain $x_0 \in (x_H, 1)$, the interglacial inertia coefficient is identically zero ($d(x_0) \equiv 0$). Furthermore, at any interior local maximum $x_0 > x_{\min}$ where $\dot{x}$ reaches zero from the retreat branch, Eq. (3) requires $u[SF(x_0 - x_H)^{-N} + cF(x_0 - x_H)] = B_1(x_0 - x_H)^{-N} + B_0$. The term in brackets is therefore identically equal to $[B_1(x_0 - x_H)^{-N} + B_0]/u > 0$ for any c. Consequently, upon switching from retreat ($u > 1$) to glaciation ($u = 1$), $\dot{x}(t^+)$ drops instantaneously to a strictly negative value:

$$\dot{x}(t^+) = -\frac{u-1}{u}\left[B_1(x_0 - x_H)^{-N} + B_0\right] < 0. \tag{D5}$$

This strict negative velocity jump proves analytically that local maxima form deterministic corners without Filippov sliding or numerical chattering at $\dot{x} = 0$, as the system is immediately driven back into the glaciating branch where $x_{\min}$ resets to x.

https://doi.org/10.5194/egusphere-2026-7112
Preprint. Discussion started: 25 November 2026
© Author(s) 2026. CC BY 4.0 License.

A discontinuity of $\mathrm{d}x/\mathrm{d}t$ is also present in Paillard (1998) at every state transition. The two models therefore differ not at turning points in general, but at the onset of a termination, where here the rate is continuous (with unbounded sensitivity to the first retreat) while in Paillard's model it jumps between two linear regimes.

Identifying the coefficient of x in Eq. (D4) with $-\tau_R^{-1}$ defines $\tau_R = -1/\mathcal{B}$, with $\mathcal{B} = \partial\dot{x}/\partial x$ evaluated at the reference point. During glaciation ($u = 1$, $c = C_1 < 0$) $\mathcal{B}$ is negative for all but the weakest insolation, so $\tau_R > 0$ and the local dynamics is a relaxation as in Paillard (1998). During retreat ($c = C_2 > 0$) the positive terms proportional to h and to $u C_2 F$ can exceed the stabilising term $-u\,N\,S\,F\,(x - x_H)^{-N-1}$, so that $\mathcal{B} > 0$ and $\tau_R < 0$: the identification then describes the e-folding time of an instability, not a relaxation. We regard this as the local expression of the runaway of a termination, which in the piecewise-linear formulation is hidden in the instantaneous switch between states.

This proves the local quasi equivalence between our model and Paillard's model, although some differences remain, which explain the different behaviour of the two models. It is likely that an equation such as Eq. 1 which accounts for further dependencies of the parameters on volume, insolation, volume-derivative sign and previous local maxima could reproduce the same results as Eq. 3.

The expansion is local. The coefficients are evaluated at a reference point $(x_0, F(t_0))$ and the cross terms $(F - F(t_0))(x - x_0)$ are neglected. The equation is exactly linear in F at fixed x, u and c, so the term multiplying F is not approximated. Consequently τ_R and x_R identified below depend on the reference point along the trajectory, $\tau_R = \tau_R(x_0, F(t_0), history)$, whereas in Paillard (1998) they are constant within each state; and the approximation is accurate only while F varies little during the time spent near x_0, which is not the case during a termination. Moreover, the expansion assumes that c, d and the retreat mode do not switch within the neighbourhood of the reference point, i.e. that F stays on one side of F_0, that x stays on one side of 1, and that $\dot{x}$ keeps its sign. The equivalence is therefore regime-wise, in the same sense in which Paillard's model is piecewise linear: our switches (c at F_0, d at $x = 1$, the retreat mode) play the role of his state transitions. We thus speak of a local quasi-equivalence, valid between switches.

As for the extension to 2Ma, both our model and Paillard's use a linear dependence on time of two parameters: for Paillard (1998), those parameters are the maximum ice volume and the truncation of insolation; for us, they are x_H, which has a similar role to the maximum ice volume, and U, which is not related to insolation, but controls the asymmetry of the glacial cycles. However, the insolation truncation in Paillard controls the sensitivity of the ice sheet to insolation, so it has an effect on the symmetry of glacial cycles. Finally, a difference between our extension and Paillard's is that we limit the linear growth from 2Ma to 800ka, whereas Paillard applies it on the whole domain. Both choices are legitimate: assuming a linear trend in the whole domain means to assume that the increase in ice volume is due to long climatic trends, such as those observed to impact the climate system on the scale of tens of million years (Rae et al., 2021; Berends et al., 2021); assuming a linear trend up to the mid-Pleistocene transition amounts to hypothesizing a form of long-term self-regulation of glacial-cycle dynamics, potentially associated with the progressive erosion of subglacial regolith (Clark and Pollard, 1998; Berends et al., 2021). By exposing bedrock, this process can favour the development of thicker ice sheets, which, consistently with the scaling relationships between ice-sheet thickness and area discussed by Bahr et al. (2015), can also be expected to have a larger area. In our model, this progressive growth is assumed to continue from one glacial cycle to the next, up to a latitudinal limit.

https://doi.org/10.5194/egusphere-2026-7112
Preprint. Discussion started: 25 November 2026
© Author(s) 2026. CC BY 4.0 License.

Appendix E: On linear temperature-dependent mass-balance formulations

A number of related conceptual models, including Pérez-Montero et al. (2025), parameterise both snowfall and ablation as linear functions of a single global (or ice-sheet-averaged) temperature T: $\mathrm{SF} = \mathrm{SF}_0 + \gamma(T - T_0^{\mathrm{SF}})$ and $A = A_0 + \beta(T - T_0^{A})$. The resulting surface mass balance is

$$SMB = \mathrm{SF} - A = (\gamma - \beta)\,T + \text{const.} \tag{E1}$$

The immediate consequence is not merely that the sign of SMB's response to T is set by $\mathrm{sign}(\gamma - \beta)$, but that SMB, which is the only quantity these models are calibrated against, constrains γ and β solely through their *difference*. Any calibration procedure that fits such a model to an ice-volume or δ^{18}O record is therefore unable to separately identify the snowfall sensitivity from the ablation sensitivity: infinitely many (γ, β) pairs sharing the same difference produce identical mass-balance histories. This is a standard equifinality problem in conceptually simple, linearly forced models (e.g., Wagener et al., 2003), and it means that any physical narrative attached individually to "snowfall response" or "ablation response" in such models — for instance, attributing a change in regime to strengthened ablation rather than weakened accumulation — is underdetermined by the data used to calibrate them, however plausible the narrative may be. It has to be said that the temperature-dependent part of the mass balance in Pérez-Montero et al. (2025) has this structure; their albedo, which depends on ice age, adds a state-dependent term that partly lifts the degeneracy.

In the present model this degeneracy is removed by a stated hypothesis, not by the calibration. Insolation F plays the role of a temperature proxy and enters linearly only in the ablation-side terms $SF(x - x_H)^{-N}$ and $cF(x - x_H)$, while B_0 and $B_1(x - x_H)^{-N}$ carry no F-dependence ($\gamma \equiv 0$ in the notation above; although a local sub-threshold dependence of buildup is contained in C_1). The terms B_0, $B_1(x - x_H)^{-N}$ and $SF(x - x_H)^{-N}$ are distinct functions of (F, x): the last two share the same dependence on x, but only $SF(x - x_H)^{-N}$ varies with F, so that at a given margin position the response of $\mathrm{d}x/\mathrm{d}t$ to insolation is attributed to S and B_1 sets the baseline. If snowfall did depend on insolation, for instance $B_1(x - x_H)^{-N}(1 + \tilde{\epsilon}F)$ (where $\tilde{\epsilon} = (S/B_1)\epsilon$ in terms of the fractional ratio ϵ defined in Sect. 2.2), then on the glaciating branch and at termination onset ($u = 1$) the calibration would constrain only the net coefficient $S - B_1\tilde{\epsilon}$, and S would have to be read as a net sensitivity (while during retreat, where $u > 1$ multiplies S but not B_1, the degeneracy holds approximately since $B_1/S \ll 1$). The effect is limited by the relative size of the two terms: with the calibrated values $B_1/S \simeq 0.024$ for the best-fit set (and $B_1/S \simeq 0.056$ for the MIS6-adaptable set), even a doubling of moisture transport over the whole range of F ($\tilde{\epsilon} \sim 1$) would shift the net coefficient by only about 2%–6%. Whether snowfall is insensitive to insolation at first order is a physical hypothesis, motivated by the thermal isolation of the ice-sheet interior, and the calibration cannot test it. The identifiability stated here concerns this split only: the ten-parameter calibration has other degeneracies, since structurally different local solutions exist (Table 1 and A3) and some parameters, such as D, are only weakly constrained; the Hessian analysis (Sect. 3.3) characterises only the neighbourhood of the selected solution.

https://doi.org/10.5194/egusphere-2026-7112
Preprint. Discussion started: 25 November 2026
© Author(s) 2026. CC BY 4.0 License.

Author contributions. EM proposed the original idea, implemented it, wrote the code and the paper. FG and CS supervised the work and proposed corrections and integrations.

Competing interests. The authors declare that they have no competing interests.

Acknowledgements. The first author used Claude (Anthropic) as an assistant for code review, language editing, drafting of parts of the text and preliminary literature search. The authors reviewed and verified all output and take full responsibility for the content of the manuscript.

https://doi.org/10.5194/egusphere-2026-7112
Preprint. Discussion started: 25 November 2026
© Author(s) 2026. CC BY 4.0 License.

References

Abe-Ouchi, A., Saito, F., Kawamura, K., Raymo, M. E., Okuno, J., Takahashi, K., and Blatter, H.: Insolation-Driven 100,000-Year Glacial Cycles and Hysteresis of Ice-Sheet Volume, Nature, 500, 190–193, https://doi.org/10.1038/nature12374, 2013.

Allen, M. R. and Ingram, W. J.: Constraints on future changes in climate and the hydrologic cycle, Nature, 419, 224–232, https://doi.org/10.1038/nature01092, 2002.

Bahr, D. B., Pfeffer, W. T., and Kaser, G.: A review of volume-area scaling of glaciers, Reviews of Geophysics, 53, 95–140, https://doi.org/10.1002/2014RG000470, 2015.

Berends, C. J., Köhler, P., Lourens, L. J., and van de Wal, R. S. W.: On the Cause of the Mid-Pleistocene Transition, Reviews of Geophysics, 59, e2020RG000 727, https://doi.org/10.1029/2020RG000727, 2021.

Berger, A.: Long-Term Variations of Daily Insolation and Quaternary Climatic Changes, Journal of the Atmospheric Sciences, 35, 2362–2367, https://doi.org/10.1175/1520-0469(1978)035<2362:LTVODI>2.0.CO;2, 1978.

Broecker, W. S.: Thermohaline circulation, the Achilles heel of our climate system: will man-made CO2 upset the current balance?, Science, 278, 1582–1588, https://doi.org/10.1126/science.278.5343.1582, 1997.

Budyko, M. I.: The effect of solar radiation variations on the climate of the Earth, Tellus, 21, 611–619, https://doi.org/10.1111/j.2153-3490.1969.tb00466.x, 1969.

Cheng, H., Edwards, R. L., Broecker, W. S., Denton, G. H., Kong, X., Wang, Y., Zhang, R., and Wang, X.: Ice age terminations, Science, 326, 248–252, https://doi.org/10.1126/science.1177840, 2009.

Clark, P. U. and Pollard, D.: Origin of the middle Pleistocene transition by ice sheet erosion of regolith, Paleoceanography, 13, 1–9, https://doi.org/10.1029/97PA02660, 1998.

Cook, J. M., Tedstone, A. J., Williamson, C., McCutcheon, J., Hodson, A. J., Dayal, A., Skiles, M., Hofer, S., Bryant, R., McAree, O., et al.: Glacier algae accelerate melt rates on the south-western Greenland Ice Sheet, The Cryosphere, 14, 309–330, https://doi.org/10.5194/tc-14-309-2020, 2020, 2020.

Cook, K. H. and Held, I. M.: Stationary Waves of the Ice Age Climate, Journal of Climate, 1, 807–819, https://doi.org/10.1175/1520-0442(1988)001<0807:swotia>2.0.co;2, 1988.

Crucifix, M.: How Can a Glacial Inception Be Predicted?, The Holocene, 21, 831–842, https://doi.org/10.1177/0959683610394883, 2011.

Crucifix, M.: Oscillators and Relaxation Phenomena in Pleistocene Climate Theory, Philosophical Transactions of the Royal Society A, 370, 1140–1165, https://doi.org/10.1098/rsta.2011.0315, 2012.

Daruka, I. and Ditlevsen, P. D.: A Conceptual Model for Glacial Cycles and the Middle Pleistocene Transition, Climate Dynamics, 46, 29–40, https://doi.org/10.1007/s00382-015-2564-7, 2016.

DeConto, R. and Pollard, D.: Contribution of Antarctica to past and future sea-level rise, Nature, 531, 591–597, https://doi.org/10.1038/nature17145, 2016.

Delaygue, G., Masson, V., Jouzel, J., Koster, R. D., and Healy, R. J.: The origin of Antarctic precipitation: a modelling approach, Tellus B, 52, 19–36, https://doi.org/10.3402/tellusb.v52i1.16079, 2000.

Ditlevsen, P. D.: Bifurcation structure and noise-assisted transitions in the Pleistocene glacial cycles, Paleoceanography, 24, https://doi.org/10.1029/2008PA001673, 2009.

Fischer, H., Wahlen, M., Smith, J., Mastroianni, D., and Deck, B.: Ice Core Records of Atmospheric CO2 around the Last Three Glacial Terminations, Science, 283, 1712–1714, https://doi.org/10.1126/science.283.5408.1712, 1999.

https://doi.org/10.5194/egusphere-2026-7112
Preprint. Discussion started: 25 November 2026
© Author(s) 2026. CC BY 4.0 License.

Ganopolski, A.: Toward generalized Milankovitch theory (GMT), Climate of the Past, 20, 151–185, https://doi.org/10.5194/cp-20-151-2024, 2024.

Ganopolski, A. and Calov, R.: Simulation of the last glacial cycle with a coupled climate ice-sheet model of intermediate complexity, Climate of the Past, 6, 229–242, https://doi.org/10.5194/cp-6-229-2010, 2010.

Ganopolski, A. and Calov, R.: The Role of Orbital Forcing, Carbon Dioxide and Regolith in 100 kyr Glacial Cycles, Climate of the Past, 7, 1415–1425, https://doi.org/10.5194/cp-7-1415-2011, 2011.

Gao, Q., Sime, L. C., McLaren, A. J., Bracegirdle, T. J., Capron, E., Rhodes, R. H., Steen-Larsen, H. C., Shi, X., and Werner, M.: Evaporative controls on Antarctic precipitation: an ECHAM6 model study using innovative water tracer diagnostics, The Cryosphere, 18, 683–703, https://doi.org/10.5194/tc-18-683-2024, 2024.

Ghil, M.: Cryothermodynamics: The Chaotic Dynamics of Paleoclimate, Physica D: Nonlinear Phenomena, 77, 130–159, https://doi.org/10.1016/0167-2789(94)90131-7, 1994.

Gildor, H. and Tziperman, E.: Sea ice as the glacial cycles' climate switch: Role of seasonal and orbital forcing, Paleoceanography, 15, 605–615, https://doi.org/10.1029/1999PA000461, 2000.

Golledge, N. R., Menviel, L., Carter, L., Fogwill, C. J., England, M. H., Cortese, G., and Levy, R. H.: Antarctic contribution to meltwater pulse 1A from reduced Southern Ocean overturning, Nature communications, 5, 5107, https://doi.org/10.1038/ncomms6107, 2014.

Hays, J. D., Imbrie, J., and Shackleton, N. J.: Variations in the Earth's Orbit: Pacemaker of the Ice Ages: For 500,000 years, major climatic changes have followed variations in obliquity and precession, Science, 194, 1121–1132, https://doi.org/10.1126/science.194.4270.1121, 1976.

Held, I. M. and Soden, B. J.: Robust Responses of the Hydrological Cycle to Global Warming, Journal of Climate, 19, 5686 – 5699, https://doi.org/10.1175/JCLI3990.1, 2006.

Huybers, P. and Wunsch, C.: Obliquity Pacing of the Late Pleistocene Glacial Terminations, Nature, 434, 491–494, https://doi.org/10.1038/nature03401, 2005.

Imbrie, J. and Imbrie, J. Z.: Modeling the Climatic Response to Orbital Variations, Science, 207, 943–953, https://doi.org/10.1126/science.207.4434.943, 1980.

Imbrie, J., Berger, A., Boyle, E., Clemens, S., Duffy, A., Howard, W., Kukla, G., Kutzbach, J., Martinson, D., McIntyre, A., et al.: On the structure and origin of major glaciation cycles 2. The 100,000-year cycle, Paleoceanography, 8, 699–735, https://doi.org/10.1029/93PA02751, 1993.

Joughin, I., Alley, R., and Holland, D.: Ice-sheet response to oceanic forcing, Science, 338, 1172–1176, https://doi.org/https://doi.org/10.1126/science.1226481, 2012.

Laskar, J., Robutel, P., Joutel, F., Gastineau, M., Correia, A. C., and Levrard, B.: A long-term numerical solution for the insolation quantities of the Earth, Astronomy & Astrophysics, 428, 261–285, https://doi.org/10.1051/0004-6361:20041335, 2004.

Legrain, E., Parrenin, F., and Capron, E.: A gradual change is more likely to have caused the Mid-Pleistocene Transition than an abrupt event, Communications Earth & Environment, 4, 90, https://doi.org/10.1038/s43247-023-00754-0, 2023.

Leloup, G. and Paillard, D.: Influence of the choice of insolation forcing on the results of a conceptual glacial cycle model, Climate of the Past, 18, 547–558, https://doi.org/10.5194/cp-18-547-2022, 2022.

Liakka, J. and Nilsson, J.: The Impact of Topographically Forced Stationary Waves on Local Ice-Sheet Climate, Journal of Glaciology, 56, 534–544, https://doi.org/10.3189/002214310792447824, 2010.

https://doi.org/10.5194/egusphere-2026-7112
Preprint. Discussion started: 25 November 2026
© Author(s) 2026. CC BY 4.0 License.

Lisiecki, L. E. and Raymo, M. E.: A Pliocene-Pleistocene Stack of 57 Globally Distributed Benthic δ^{18}O Records, Paleoceanography, 20, PA1003, https://doi.org/10.1029/2004PA001071, 2005.

Maasch, K. A. and Saltzman, B.: A Low-Order Dynamical Model of Global Climatic Variability over the Full Pleistocene, Journal of Geophysical Research, 95, 1955–1963, https://doi.org/10.1029/JD095iD02p01955, 1990.

Maiero, E., Giorgi, F., and Solidoro, C.: 1-ODE conceptual model of glacial-interglacial cycles driven by 65N insolation (v1.0.2), https://doi.org/10.5281/zenodo.24165064, https://doi.org/10.5281/zenodo.24165064, 2026.

Milanković, M.: Kanon der Erdbestrahlung und seine Anwendung auf das Eiszeitenproblem, http://elibrary.matf.bg.ac.rs/handle/123456789/702, special Publication 132, 1941.

Miller, K. G., Browning, J. V., Schmelz, W. J., Kopp, R. E., Mountain, G. S., and Wright, J. D.: Cenozoic sea-level and cryospheric evolution from deep-sea geochemical and continental margin records, Science advances, 6, eaaz1346, https://doi.org/10.1126/sciadv.aaz1346, 2020.

Monnin, E., Indermühle, A., Dällenbach, A., Flückiger, J., Stauffer, B., Stocker, T. F., Raynaud, D., and Barnola, J.-M.: Atmospheric CO2 Concentrations over the Last Glacial Termination, Science, 291, 112–114, https://doi.org/10.1126/science.291.5501.112, 2001.

Oerlemans, J.: Model experiments on the 100,000-yr glacial cycle, Nature, 287, 430–432, https://doi.org/10.1038/287430a0, 1980.

Oerlemans, J., Giesen, R., and Van Den Broeke, M.: Retreating alpine glaciers: increased melt rates due to accumulation of dust (Vadret da Morteratsch, Switzerland), Journal of Glaciology, 55, 729–736, https://doi.org/10.3189/002214309789470969, 2009.

Paillard, D.: The timing of Pleistocene glaciations from a simple multiple-state climate model, Nature, 391, 378–381, https://doi.org/10.1038/34891, 1998.

Paillard, D. and Parrenin, F.: The Antarctic Ice Sheet and the Triggering of Deglaciations, Earth and Planetary Science Letters, 227, 263–271, https://doi.org/10.1016/j.epsl.2004.08.023, 2004.

Parrenin, F. and Paillard, D.: Amplitude and phase of glacial cycles from a conceptual model, Earth and Planetary Science Letters, 214, 243–250, https://doi.org/10.1016/S0012-821X(03)00363-7, 2003.

Parrenin, F., Masson-Delmotte, V., Köhler, P., Raynaud, D., Paillard, D., Schwander, J., Barbante, C., Landais, A., Wegner, A., and Jouzel, J.: Synchronous Change of Atmospheric CO2 and Antarctic Temperature during the Last Deglacial Warming, Science, 339, 1060–1063, https://doi.org/10.1126/science.1226368, 2013.

Paul, F., Kääb, A., Maisch, M., Kellenberger, T., and Haeberli, W.: Rapid disintegration of Alpine glaciers observed with satellite data, Geophysical research letters, 31, https://doi.org/10.1029/2004GL020816, 2004.

Pérez-Montero, S., Alvarez-Solas, J., Swierczek-Jereczek, J., Moreno-Parada, D., Robinson, A., and Montoya, M.: A simple physical model for glacial cycles, Earth System Dynamics, 16, 915–937, https://doi.org/10.5194/esd-16-915-2025, 2025.

Pierrehumbert, R. T.: Principles of planetary climate, vol. 10, Cambridge University Press, https://doi.org/10.1017/CBO9780511780783, 2010.

Quinn, C., Sieber, J., von der Heydt, A. S., and Lenton, T. M.: The Mid-Pleistocene Transition induced by delayed feedback and bistability, Dynamics and Statistics of the Climate System, 3, dzy005, https://doi.org/10.1093/climsys/dzy005, 2018.

Rae, J. W., Zhang, Y. G., Liu, X., Foster, G. L., Stoll, H. M., and Whiteford, R. D.: Atmospheric CO2 over the past 66 million years from marine archives, Annual Review of Earth and Planetary Sciences, 49, 609–641, https://doi.org/10.1146/annurev-earth-082420-063026, 2021.

Rahmstorf, S.: Ocean circulation and climate during the past 120,000 years, Nature, 419, 207–214, https://doi.org/10.1038/nature01090, 2002.

https://doi.org/10.5194/egusphere-2026-7112
Preprint. Discussion started: 25 November 2026
© Author(s) 2026. CC BY 4.0 License.

Ren, S., Jia, L., Miles, E. S., Menenti, M., Kneib, M., Shaw, T. E., Buri, P., McCarthy, M. J., Yang, W., Pellicciotti, F., et al.: Observed and projected declines in glacier albedo across the Third Pole in the 21st century, One Earth, 7, 1587–1599, https://doi.org/10.1016/j.oneear.2024.08.010, 2024.

Roe, G. H. and Lindzen, R. S.: The Mutual Interaction between Continental-Scale Ice Sheets and Atmospheric Stationary Waves, Journal of Climate, 14, 1450–1465, https://doi.org/10.1175/1520-0442(2001)014<1450:TMIBCS>2.0.CO;2, 2001.

Rohling, E., Foster, G. L., Grant, K., Marino, G., Roberts, A., Tamisiea, M. E., and Williams, F.: Sea-level and deep-sea-temperature variability over the past 5.3 million years, Nature, 508, 477–482, https://doi.org/10.1038/nature13230, 2014.

Saltzman, B. and Maasch, K. A.: Carbon Cycle Instability as a Cause of the Late Pleistocene Ice Age Oscillations: Modeling the Asymmetric Response, Global Biogeochemical Cycles, 2, 177–185, https://doi.org/10.1029/GB002i002p00177, 1988.

Shakun, J. D., Clark, P. U., He, F., Marcott, S. A., Mix, A. C., Liu, Z., Otto-Bliesner, B., Schmittner, A., and Bard, E.: Global Warming Preceded by Increasing Carbon Dioxide Concentrations during the Last Deglaciation, Nature, 484, 49–54, https://doi.org/10.1038/nature10915, 2012.

Shaw, T. E., Ulloa, G., Farías-Barahona, D., Fernandez, R., Lattus, J. M., and McPhee, J.: Glacier albedo reduction and drought effects in the extratropical Andes, 1986–2020, Journal of Glaciology, 67, 158–169, https://doi.org/10.1017/jog.2020.102, 2021.

Shimada, R., Takeuchi, N., and Aoki, T.: Inter-annual and geographical variations in the extent of bare ice and dark ice on the Greenland ice sheet derived from MODIS satellite images, Frontiers in Earth Science, 4, 43, https://doi.org/doi.org/10.3389/feart.2016.00043, 2016.

Sodemann, H. and Stohl, A.: Asymmetries in the moisture origin of Antarctic precipitation, Geophysical research letters, 36, https://doi.org/10.1029/2009GL040242, 2009.

Sodemann, H., Masson-Delmotte, V., Schwierz, C., Vinther, B., and Wernli, H.: Interannual variability of Greenland winter precipitation sources: 2. Effects of North Atlantic Oscillation variability on stable isotopes in precipitation, Journal of Geophysical Research: Atmospheres, 113, https://doi.org/10.1029/2007JD009416, 2008.

Spratt, R. M. and Lisiecki, L. E.: A Late Pleistocene sea level stack, version 2, https://doi.org/10.1594/PANGAEA.979830, 2025.

Stommel, H.: Thermohaline convection with two stable regimes of flow, Tellus, 13, 224–230, https://doi.org/10.1111/j.2153-3490.1961.tb00079.x, 1961.

Stone, P. H.: Constraints on dynamical transports of energy on a spherical planet, Dynamics of atmospheres and oceans, 2, 123–139, https://doi.org/10.1016/0377-0265(78)90006-4, 1978.

Stouffer, R. J. et al.: Investigating the causes of the response of the thermohaline circulation to past and future climate changes, Journal of Climate, 19, 1365–1387, https://doi.org/10.1175/JCLI3689.1, 2006.

Talento, S. and Ganopolski, A.: Reduced-complexity model for the impact of anthropogenic CO2 emissions on future glacial cycles, Earth System Dynamics, 12, 1275–1293, https://doi.org/10.5194/esd-12-1275-2021, 2021.

Tedesco, M., Doherty, S., Fettweis, X., Alexander, P., Jeyaratnam, J., and Stroeve, J.: The darkening of the Greenland ice sheet: trends, drivers, and projections (1981–2100), The Cryosphere, 10, 477–496, https://doi.org/doi.org/10.5194/tc-10-477-2016, 2016.

Tzedakis, P., Crucifix, M., Mitsui, T., and Wolff, E. W.: A simple rule to determine which insolation cycles lead to interglacials, Nature, 542, 427–432, https://doi.org/10.1038/nature21364, 2017.

Tziperman, E. and Gildor, H.: On the mid-Pleistocene transition to 100-kyr glacial cycles and the asymmetry between glaciation and deglaciation times, Paleoceanography, 18, 1–1, https://doi.org/10.1029/2001pa000627, 2003.

Verbitsky, M. Y. and Crucifix, M.: Do phenomenological dynamical paleoclimate models have physical similarity with Nature? Seemingly, not all of them do, Climate of the Past, 19, 1793–1803, https://doi.org/10.5194/cp-19-1793-2023, 2023.

https://doi.org/10.5194/egusphere-2026-7112
Preprint. Discussion started: 25 November 2026
© Author(s) 2026. CC BY 4.0 License.



Wagener, T., McIntyre, N., Lees, M. J., Wheater, H. S., and Gupta, H. V.: Towards Reduced Uncertainty in Conceptual Rainfall-Runoff Modelling: Dynamic Identifiability Analysis, Hydrological Processes, 17, 455–476, https://doi.org/10.1002/hyp.1135, 2003.

Whitehouse, P. L.: Glacial isostatic adjustment modelling: historical perspectives, recent advances, and future directions, Earth Surface Dynamics, 6, 401–429, https://doi.org/10.5194/esurf-6-401-2018, 2018.

Willeit, M., Ganopolski, A., Calov, R., and Brovkin, V.: Mid-Pleistocene Transition in Glacial Cycles Explained by Declining CO2 and Regolith Removal, Science Advances, 5, eaav7337, https://doi.org/10.1126/sciadv.aav7337, 2019.